GATA1 pathogenic variants disrupt MYH10 silencing during megakaryopoiesis

Paul Saultier, Sandrine Cabantous, Michel Puceat, Franck Peiretti, Timothée Bigot, Noémie Saut, Jean-claude Bordet, Matthias Canault, Johannes Agthoven, Marie Loosveld, et al.

GATA1 pathogenic variants disrupt MYH10 silencing during megakaryopoiesis.

Paul Saultier,[1,2] Sandrine Cabantous,[1] Michel Puceat,[3] Franck Peiretti,[1] Bigot Timothée,[1] Noémie Saut,[1,4] Jean-Claude Bordet,[5] Matthias Canault,[1] Johannes van Agthoven,[6] Marie Loosveld,[4,7] Dominique Payet-Bornet[7], Delphine Potier[7], Céline Falaise,[2,4] Denis Bernot,[1] Pierre Emmanuel Morange,[1,4] Marie-Christine Alessi,[1,4 *] and Marjorie Poggi[1]

[1]Aix Marseille Univ, INSERM, INRAe, C2VN, Marseille, France

[2]APHM, La Timone Children's Hospital, Department of pediatric hematology, immunology and oncology, Marseille, France

[3]Aix Marseille Univ, INSERM, MMG, Marseille, France

[4]APHM, CHU Timone, French Reference Center on Inherited Platelet Disorders, Marseille, France

[5]Unité d'Hémostase Biologique, Bron, France

[6]Structural Biology Program, Division of Nephrology/Department of Medicine, Massachusetts General Hospital and Harvard Medical School, Charlestown, MA 02129, USA

[7]Aix-Marseille Univ, CNRS, INSERM, CIML, Marseille, France.

*__Corresponding author__ : Marie-Christine Alessi, C2VN, Faculté de Médecine Timone, 27 Boulevard Jean Moulin, 13385 Marseille, France ; E-mail : marie-christine.alessi@univ-amu.fr ; Tel : +33 491 324 507 ; Fax : +33 491 254 336.

Abstract: 238 words

Text: 5002 words

Figures: 5

Tables: 3

Supporting Information: 9 figures and 2 tables

References: 41

Abstract

Background

GATA1 is an essential transcription factor for both polyploidization and megakaryocyte (MK) differentiation. The polyploidization defect observed in *GATA1* variant carriers is not well understood.

Objective

To extensively phenotype two pedigrees displaying different variants in the *GATA1* gene and determine if GATA1 controls MYH10 expression levels, a key modulator of MK polyploidization.

Method

146 unrelated *propositi* with constitutional thrombocytopenia were screened on a multigene panel. We described the genotype-phenotype correlation in GATA1 variant carriers and investigated the effect of these novel variants on MYH10 transcription using luciferase constructs.

Results

The clinical profile associated with the p.L268M variant localized in the C terminal Zinc finger was unusual in that the patient displayed bleeding and severe platelet aggregation defects without early-onset thrombocytopenia. p.N206I localized in the N terminal Zinc finger was associated, on the other hand, with severe thrombocytopenia (15G/L) in early life. High *MYH10* levels were evidenced in platelets of GATA1 variant carriers. Analysis of MKs anti-GATA1 ChIP-sequencing data revealed two GATA1 binding sites, located in the 3' untranslated region and in intron 8 of the *MYH10* gene. Luciferase reporter assays showed their respective role in the regulation of MYH10 gene expression. Both GATA1 variants significantly alter intron 8 driven MYH10 transcription.

Conclusion

The discovery of an association between MYH10 and GATA1 is a novel one. Overall, this study suggests that impaired *MYH10* silencing via an intronic regulatory element is the most likely cause of GATA1-related polyploidization defect.

Key words

GATA1, MYH10, downstream targets, functional variants, platelets.

Essentials

- MYH10 silencing is an essential step in the megakaryocyte polyploidization.
- Two novel GATA1 variants were identified in the N and C-terminal zinc finger domain.
- MYH10 expression levels are increased in platelets from both GATA1 variant carriers.
- GATA1 alters MYH10 expression via an intronic binding site in the MYH10 gene.

Main Text

Introduction

GATA1 is an essential transcription factor for erythrocyte and megakaryocyte (MK) differentiation [1,2]. It belongs to the GATA family of zinc finger (ZF) transcription factors, which recognize the W(A/T)GATAR(A/G) DNA pattern. The protein is encoded by the *GATA1* gene, located on the X chromosome [3,4]. The GATA1 protein contains two highly conserved ZFs, which are separated by a short linker. The C-terminal ZF binds with high affinity and specificity to (A/T)GATA(A/G) motifs throughout the genome, while the N-terminal ZF can bind protein cofactors, such as FOG1.

Several hemizygous loss-of-function *GATA1* variants have been described in patients with varying degrees of macrothrombocytopenia and anemia. Most of these variants affect the N-terminal ZF of GATA1 and impair the GATA1 DNA binding interaction with the GATA1 cofactor FOG1 [5–7]. Accordingly, mice with targeted mutations in the *Gata1* promoter display macrothrombocytopenia, in which reduced Gata1 expression [8–10] or conditional knockout of *Gata1* results in a selective loss of Gata1 expression in MKs [11]. This observation underscores the importance of GATA1 in sustaining normal megakaryocytic differentiation and platelet production. Previous studies have shown that *GATA1* is required for both polyploidization and MK differentiation. Bone marrow from *GATA1* variant carriers shows a moderate to marked increase in MK numbers, which are also small and hypolobulated [5,6].*In vivo*, the Gata1^{low} mice display a marked increase in small and hypoploid MKs [9]. GATA1-deficient MKs also exhibit increased proliferation both *in vitro* and *in vivo* with defective nuclear and cytoplasmic maturation [9,10].

Some studies have suggested that the polyploidization defect is associated with GATA1 inactivation through deregulation of cyclin D1, STAT1 or CDC6 expression [10,12]. However, we propose an alternative mechanism involving altered silencing of the protein non-muscle heavy chain IIB (MYH10). During polyploidization, expression of MYH10 protein, which localizes to the actomyosin contractile ring, is repressed by the transcription repressor RUNX1, thereby enabling the switch from mitosis to endomitosis [13]. The polyploidization defect observed in *RUNX1* variant carriers is in part associated with the persistence of MYH10 expression [14], which has been detected in circulating platelets [15].

Similarly, increased levels of MYH10 protein have been detected in platelets from patients carrying *FLI1* variants, thus suggesting cooperation between the two transcription factors, RUNX1 and FLI1, in normal repression of the *MYH10* gene [15–18].

Genome-wide analysis of simultaneous GATA1, RUNX1, FLI1 and TAL1 DNA binding in human MKs has revealed that these transcription factors bind to the same binding sites in the genome and cooperate to regulate the expression of target genes during the early stages of megakaryopoiesis [19]. Transcriptional cooperation between RUNX1 and GATA1 in the activation of megakaryocytic promoters has been further established using reporter assays with transient transfection in a variety of mammalian cell lines. These studies have demonstrated the physical interaction between the two transcription factors [20,21]. Therefore, we suggest that deregulation of *MYH10* expression may also be implicated in *GATA1*-related thrombocytopenia.

In this study, we report a detailed analysis of two novel GATA1 variants localized in each ZF. Elevated MYH10 protein levels were found in platelets from carriers of each variant. We describe the identification of a *MYH10* intronic region that functions as a GATA1-responsive cis-regulatory element.

Materials and Methods

Methods concerning high-throughput gene sequencing, structural model of GATA1-DNA interactions, flow cytometry analysis, cell expression and luciferase reporter assays, platelet-rich plasma (PRP) serotonin level, platelet PAI-1 level, mepacrine uptake and release, immunoprecipitation and western blot analysis, and epifluorescence microscopy are described in the Online Supplementary Material. *Study limitations:* Owing to the limited number of patients, statistical comparison between patients and controls was not always possible. Fresh whole blood (required for primary cell culture) was available in only one patient (F1-II1). Consequently, most in vitro experiment was performed using transfected non-hematopoietic cell line. The platelet serotonin levels were available for two patients and the BM smears for one patient. TEM analysis of platelets were performed for only one family. The others experiments were performed for all the patients.

Patient enrollment, research ethics, patient consent, and clinical and laboratory data

From 2014 to 2017, we recruited 146 unrelated *propositi* with constitutional thrombocytopenia of unknown origin. Genetic analyses were performed at the French Reference Center for Inherited Platelet Disorders at La Timone University Hospital in Marseille, France. All cases were included in the study after obtaining informed written consent in accordance with protocols approved by national institutional review boards and the Declaration of Helsinki principles. Medical and family history data were obtained from medical reports and patient interviews. Bleeding tendency was assessed using the International Society on Hemostasis and Thrombosis-Bleeding Assessment Tool (ISTH-BAT) score. Red blood cell counts, platelet counts, mean corpuscular volume (MCV) and mean platelet volume (MPV) were determined on EDTA-anticoagulated blood samples using the ADVIA 120 automated cell counter. Bone marrow smears were obtained for one propositus and stained with May-Grünwald-Giemsa. Fetal hemoglobin levels were assessed using high-performance liquid chromatography in the Biochemistry Department at La Timone University Hospital in Marseille, France.

Platelet aggregation

Platelet aggregation was assessed by measuring light transmission through the stirred platelet-rich plasma (PRP) suspensions for 3 min using an APACT 4004 aggregometer. Platelet aggregation was triggered by adding 1 µM or 2.5 µM adenosine diphosphate (ADP; Helena laboratories), 0.5 mg/ml arachidonic acid (Helena laboratories) and 0.36 µg/ml or 0.72 µg/ml collagen (Bio/Data Corporation). Platelet agglutination was triggered by adding 1.5 mg/ml ristocetin (Sigma-Aldrich).

Evaluation of platelet granules using electron microscopy

Transmission electron microscopy (TEM) analysis of platelets was performed as previously described [18]. Briefly, we assessed platelet surface area (μm^2) and diameter (µm), the number of alpha granules per unit area (μm^{-2}), and the diameter of alpha granules in a blinded case/control experiment. Dense granules were quantified using whole-mount electron microscopy as previously described [18].

In vitro megakaryocyte differentiation and ploidy

After density gradient separation (Eurobio), circulating $CD34^+$ cells were purified using positive selection with magnetic beads (Miltenyi-Biotec) and cultured in StemSpan Serum-Free Expansion Medium II supplemented with Megakaryocyte Expansion Supplement (Stemcell Technologies). At days 9 and 11 of culture, MKs were analyzed via flow cytometry for CD41 and CD42a markers (anti-CD41-APC and anti-CD42a-PE antibodies, BD Biosciences) as well as for DNA ploidy using Hoechst-33342 (Sigma-Aldrich). The cells were then analyzed using a Navios cytometer (Beckman Coulter).

Statistical analyses

Quantitative variables are expressed as the mean ± standard error. Analyses were performed using GraphPad Prism software. Statistical differences were determined via ANOVA with Dunnett's multiple comparison test. $P<0.05$ was considered statistically significant.

Results

Two novel *GATA1* variants identified via genetic analysis

Next-generation sequencing yielded the identification of two novel *GATA1* variants (NM_002049) in three boys from two unrelated families (Figures 1A-B). For the first family, only one hemizygous variant c.617A>T (p.N206I) causing alteration in the N-terminal ZF was evidenced in the proband (II-1) (Fig 1A). For the second family only one deleterious variant c.802C>A (p. L268M) was shared by the two brothers in the C terminal ZF GATA1 domain. Five other variants worn by the two brothers have been identified. None of them were pathogenic due to benign *in silico* prediction and/or high allelic frequency (>10^{-4}) in general population databases (Supplemental Table 1). The analysis of the coverage of these genes was also not in favor of deletion or duplication (data not shown). These two missense variants were absent from the GnomAD and ExAC databases, and have a Combined Annotation Dependent Depletion (CADD) score of 24.9 for c.617A>T (Request: Chromosome X, Position 48792341, CADD GRCh38-v1.6) and 23.7 for c.802C>A (Request: Chromosome X, Position 48793229, CADD GRCh38-v1.6). The chart prediction for these two variants based on different prediction tools to identify disease relevant non-synonymous single nucleotide variants is given in supplementary figure (Supplemental Figure 1A and B). The variants occurred in both mothers, while as expected, the two fathers were homozygous for wild type genotypes (Figure 1A).

Structural modeling

Structural analysis provided further insight into the mechanisms by which these two variants may exert deleterious effects. An initial sequence alignment of GATA1 orthologs and paralogs revealed that both variants affect highly conserved sequences and may therefore play a structural role in GATA1 binding to target DNA sequences or protein binding partners (Supplemental Figure 1). As shown in the X-ray structure of GATA1 in complex with double-stranded DNA, the L268 residue is located in the interface between GATA1 and the major groove of the DNA-binding sequence TGATAA (Figure 1D, left), making van der Waals contact with bases 32T, 33T, 9T and 10C (distance cutoff of 4Å). Structural modeling of the p.L268M substitution did not reveal any steric hindrance at the GATA1-

DNA interface. However, the loss-of-function effect of p.L268M likely results from distorted hydrophobic packing with the aforementioned bases (shown in the left inset of Figure 1D).

Although the N206 residue is not localized within the GATA1-DNA interface (Figure 1D, left), the p.N206I substitution may affect the capacity of GATA1 to bind to FOG1. The nuclear magnetic resonance structures of the GATA1-FOG1 complex revealed that the N206 residue is part of the interface between the two proteins, forming a specific amino-π interaction between the GATA1 side chain amino group and the aromatic ring of FOG1-Y30 (Figure 1D, right). Structural modeling showed that this interaction is disrupted in the N2016I variant. The variant caused destabilization of the GATA1/FOG1 interface by steric hindrance, likely resulting in FOG1-mediated loss of function (shown in the right inset of Figure 1D).

Nuclear localization and FOG1 binding in GATA1 cases

To further investigate the subcellular localization of the GATA1 variants, we expressed the wild-type and variant forms of GATA1 in MSR and H9C2 cells. GATA1 variants did not reduced GATA1 protein levels (data not shown). The GATA1 variants entered the nucleus to the same extent as wild-type GATA1 (Supplemental Figure 2A), thereby suggesting that the variants alter GATA1 binding properties to chromatin rather than subcellular localization. The structural prediction was confirmed via GATA1 co-immunoprecipitation using MSR cells overexpressing GATA1 (WT or variants) and FOG1. FOG1 was detected in the GATA1 precipitates of wild-type and p.L268M GATA1-expressing cells, while FOG1 detection was markedly reduced in the p.N206I GATA1 precipitates (Supplemental Figure 2B).

Case descriptions

Thrombocytopenia onset kinetics markedly differed between the two families. Thrombocytopenia was present early in life in the p.N206I carrier (F1-II-1) with a severely reduced platelet count (15 G/L) at the age of 18 months that persisted. Bleeding during dental avulsion was prevented by platelet concentrate transfusion prior to the procedure. The patient was referred to our reference center on platelet disorders because of resistance to immunoglobulin, corticosteroids and mycophenolate mofetil treatment, as immune thrombocytopenia was initially suspected. The F1 proband did not suffer

from anemia (hemoglobin 118 g/L at seven years of age), and his mean corpuscular volume was rather low (76.8 fL- normal range: 80-95 fL). May-Grunwald-Giemsa staining of bone marrow smears showed mild dyserythropoiesis with erythroblastosis and nuclear karyorrhexis (Figure 2C).

By contrast, thrombocytopenia was initially absent in the two F2 brothers carrying the p.L268M variant. At 18 and 9 months of age, F2-II-1 and F2-II-2 exhibited normal platelet counts (261 G/L and 233 G/L), respectively despite pronounced mucocutaneous bleedings. The initial hemostasis assessment in the two children showed no defects in coagulation (normal prothrombin and activated partial thromboplastin times, normal levels of the factors VIII, XIII, fibrinogen and von Willebrand factor) or fibrinolysis (normal alpha2 antiplasmin, t-PA and plasma PAI-1 levels and normal von Kaulla test) (data not shown). Bleeding time was prolonged (>15 min) and was not corrected by DDAVP injection. A severe platelet aggregation defect was detected in both brothers with normal platelet counts in PRP samples (338-380G/L). On several occasions (6 times for the older brother and 3 times for the younger brother) and in the absence of medication, collagen, arachidonic acid and TXA2 agonist U-46619 failed to induce platelet aggregation. Reduced platelet aggregation was also observed in response to ADP, while ristocetin-induced agglutination was almost normal (Table 1 and Supplemental Figure 3). Both boys were diagnosed with hereditary platelet dysfunction. Diagnosis of Glanzmann thrombasthenia has been evoked but platelet exploration has refuted it. Indeed, platelet aggregation was only slightly reduced upon stimulation with high doses ADP (10 µM) and TRAP-14 (50 µM). Exploration of GPIIbIIIa with flow cytometry showed a normal expression level of GPIIbIIIa (Table 2) and a significant increment of PAC-1 fixation after 10 µM ADP stimulation (MFI: basal state= 0.31 (normal value 0.21-0.49) stimulated state =6.23 (normal value: 5.4-16.2), positive cell: basal state= 0% (normal value <5%), stimulated state =73% (normal value >70%)). In addition, we did not detect variations, deletion or duplication in the *ITGA2B* and *ITGB3* genes and in genes involved in its activation (*FERMT3, RASGRP2, TLN1*). The altered aggregation profiles was not due to defective expression of GPVI, SYK, PLCγ2 or COX1 in platelets, with no major differences in signal intensity between the two parents and the children. A 30% reduction in TBXAS1 levels was obseverd in both F2 children compared to their parents (Supplemental Figure 4). In patient F2-II-2, dental avulsions

and an appendectomy were performed after platelet concentrate transfusions without hemorrhagic complications. At five years of age, the platelet counts for patient F2-II-1 remained in the normal range (194 x 10^9 /L), while his brother's platelet counts started to decrease at three years of age (131 x 10^9/L). Thrombocytopenia then gradually developed over time in both brothers, with more severe thrombocytopenia in the younger boy (F2-II-2) (Figure 2A). TEM analysis of platelets derived from patient F2-II-1 showed that, in keeping with previous measurements of mean platelet volume obtained using hematology analyzers, the platelet size distribution was normal (Figure 3B and Supplemental Table).

As GATA1 is critical for erythropoiesis, we also aimed to identify any red blood cell defects. Examination of peripheral F2-II-2 blood smears demonstrated abnormally shaped red blood cells with anisocytosis and poikilocytosis (Figure 2B). The F2 probands did not suffer from anemia either, with hemoglobin levels at 111 and 112 g/L at five years of age and 146 and 144 g/L at the date of last follow-up (at 27 and 23 years of age, respectively). Hemoglobin electrophoresis revealed, as already reported in several GATA1 related diseases, an elevated level of fetal hemoglobin. They both presented with elevated fetal hemoglobin levels (25%), albeit without microcytosis (MCV: 87-92 fL between five and eight years of age) and hypochromia (mean corpuscular hemoglobin concentration: 330-331 g/L between five and eight years of age). Remarkably, the two F2 brothers displayed a progressive increase in MCV over time, while their platelet counts gradually decreased (Figure 2A); the values at last follow-up were 99 and 103 fL (at 26 and 23 years of age, respectively). Table 3 resumes main characteristics of GATA1 variant carriers.

Platelets from GATA1 cases present severe dense granular defect

Electron microscopy revealed a major delta granular deficit in GATA1 variant carriers. Analysis via whole-mount electron microscopy revealed reduced numbers of dense granules, with an average of 0.44 ± 1.02 (F1-II-1), 0.56 ± 0.97 (F2-II-1) and 0.13 ± 0.49 (F2-II-2) dense granules per platelet (normal values: 5.46 ± 3.91). Furthermore, 77% (F1-II-1), 65% (F2-II-1) and 90% (F2-II-2) of platelets lacked dense granules (Figure 3A). Mepacrine uptake and release upon TRAP-14 stimulation (40 µM) and quantification of mepacrine-labeled dense granules via fluorescent microscopy confirmed

the dense granule defect in all variant carriers (Supplemental Figure 5). On several occasions, we observed low platelet serotonin levels for the two F2 brothers (F2-II-1: 0.12 µg/109 platelets in 2015, 0.10 µg/109 platelets in 2009 and F2-II-2: 0.16 µg/109 platelets in 2015, normal range: 0.3-1.2 µg/109 platelets). Flow cytometry showed reduced expression levels of the dense granule marker CD63 upon TRAP-14 stimulation in all variant carriers (Table 2).

Platelet count (Table 1), platelet aggregation (Supplemental Figure 3), flow cytometric evaluation of mepacrine uptake and release (not shown) and platelet serotonin levels (0.39 µg/109 platelets, normal range: 0.3-1.20 µg/109 platelets) were normal in the mother (F2-I-1).

Platelets from GATA1 cases present mild alpha granular defect and structural abnormalities

Assessment of peripheral blood smears from F1-II-1 and F2-II-2 did not show gray platelets, although an experienced hematologist identified some hypogranular platelets in both children (Figure 2B). Quantitative morphometric evaluation of F2-II-1 alpha granules indicated a distinct decrease in alpha granule density and consequently a decrease in the alpha granule area: total platelet area ratio (4.1%, reference range 11.0-13.5%). The diameter of the alpha granules was only slightly decreased. The platelets presented many other structural anomalies. Platelet sections showed highly variable granular and mitochondrial content, with large areas of membrane complexes that in some cases occupied the entire section (See Figure 3B legend for complete description). To further assess the alpha granules, we evaluated the levels of PAI-1 antigen in serum. Indeed, 95% of circulating PAI-1 is localized in platelets 4. Furthermore, proteomic analysis has found that reduced PAI-1 levels is a feature of gray platelet syndrome5. For the three patients, PAI-1 levels were in the normal range (F1-II-1: 0.35, F2-II-1: 0.76 and F2-II-2: 0.69, normal range 0.33-1.07 ng/106 platelets). Flow cytometry showed moderate decrease in the levels of the alpha granule protein marker CD62P upon TRAP-14 stimulation in both the F2 children's whereas CD62P did not change after TRAP-14 stimulation in the F1-II-1 (Table 2).

GATA1 variants are associated with abnormal megakaryocyte maturation and polyploidization.

Microscopic evaluation of bone marrow aspirate smears from patient F1-II-1 showed normal numbers of MKs with a high proportion of round or hypolobulated polyploid nuclei (Figure 2C) indicating abnormal maturation. We further analyzed MK development using blood-derived $CD34^+$ stem cells. The F1 carriers exhibited a 12- to 48-fold increase in circulating $CD34^+CD38^+CD45^{low}CD19^{low}$ cells (n = 2) compared with healthy controls (n = 5) (Figure 4A). Analysis of $CD41^+$ and $CD42a^+$ cells at days 9 and 11 revealed a marked reduction in MK differentiation with reduced cell size compared with two controls (Figures 4B-C). The $CD41^+CD42a^+$ population was almost absent in the F1-II-1 cells (Figure 4B). Furthermore, the percentage of high-ploidy cells (≥ 4n) in the F1-II-1 sample was reduced at day 9. The relative frequencies of 2n, 4n, 8n and 16n ploidy MKs were 54-58%, 23-27%, 4-8% and 1-2% in the controls, versus 66%, 18%, 0% and 0% in the patient carrying the GATA1 variant, respectively (Figure 4D). Bone marrow smears and MK cultures were not available for the F2 family.

GATA1 cases display increased MYH10 levels in platelets

To further investigate the effect of the *GATA1* variants on MYH10, which is required for MK polyploidization and maturation, MYH10 levels were assessed in platelets derived from patients and healthy subjects. MYH10 protein was not detected in healthy donor platelets via immunoblotting. By contrast, MYH10 expression was detected in platelets from the three probands and one carrier of a *FLI1* variant as previously reported [18]. MYH10 protein was also present in the mother of the F2 probands (F2-I-1), albeit at relatively reduced levels (Figure 4E). The polyploidization defect has been shown associated through deregulation of cyclin D1-Cdk4 or CDC6 expression [10,12]. In MSR cells, GATA1 wild-type or mutants' transfection did not altered their expression levels (Supplemental figure 6).

Evidence of a *MYH10* intronic regulatory region

Our data suggests that GATA1 regulates *MYH10* expression. Therefore, we obtained GATA1, RUNX1, and FLI1 ChIP-sequence data on primary human MKs (deposited by the Göttgens laboratory) from the Gene Expression Omnibus (GEO) database [19]. The peak enrichments on

chromosome 17, which includes the *MYH10* locus, were extracted and displayed in the UCSC genome browser. This analysis showed two enriched binding regions for the GATA1, RUNX1, and FLI1 transcription factors in the *MYH10* gene (displayed from ENCODE data using the erythroleukemia K562 cell line known to express GATA1) (Figure 5A).

The first binding peak (Chr. 17: 8472947-8473157) located in the *MYH10* 3'UTR corresponded to GATA1 and RUNX1 binding sites. Remarkably, sequence analysis did not retrieve the consensus GATA1 binding motif in this region. The second peak (Chr. 17: 8553047-8553739) was located within an intronic region and contained potential binding sites for GATA1, FLI1 and RUNX1. Four potential GATA1 binding sites (referred to as BS-1, BS-2, BS-3 and BS-4) were identified, of which three contain the reverted sequence TATC (BS-2, BS-3 and BS-4) (Supplemental Figure 7). We also uploaded the chromatin interaction analysis with paired-end tag sequencing data for CTCF and POL2 performed on the K562 cell line from ENCODE, using the UCSC genome browser. This analysis revealed that the intronic enhancer was indeed not occupied by Pol2 or CTCF (data not shown). The interaction between gene regulatory regions (displayed with data from ENCODE) revealed that the intronic site was likely within a close chromatin region in a DNA repressive loop between two CTCF enriched regions (data not shown).

Transcriptional activity of the *MYH10* intronic element

We compared the 3'UTR and intronic regulatory element-driven expression of *MYH10* using a luciferase reporter assay in two cell lines expressing or not the GATA1 hematopoietic partners. The HEL cell line expresses the GATA1, RUNX1 and FLI1 transcription factors. In HEL cells, both the 3'UTR and intronic regions significantly repressed luciferase expression compared with the pGL3 empty vector (control) (Figure 5B). Removal of only one of the four GATA1 binding sites in MYH10 intron 8 region was sufficient to yield markedly reduced intronic activity.

We then look at the effect of GATA1 variant on intron 8 driven MYH10 expression. Since HEL cells express endogenous GATA1 we used a non-hematopoietic model, the MSR epithelial cells which do not express basal levels of GATA1, RUNX1 and FLI1 (Supplemental Figure 7). In this model wild-type GATA1 transfection enhanced luciferase activity via the MYH10 intronic region (Figure 5C left),

but not via the 3'UTR region (Figure 5C right). Disruption of all four GATA binding sites in the intronic region yielded a significant reduction in luciferase activity (approximately 40%). Disruption of BS-2 (M2) or BS-4 (M4) also led to a significant reduction in luciferase activity, while disruption of BS-1 (M1) or BS-3 (M3) did not exhibit any significant effect (Figure 5C left).

We then evaluated the variants effects in MSR cells. Both here reported (N206L and L268M GATA1) and already described (V205M and G208S) GATA1 variants were associated with a marked reduction in transcriptional activity compared with wild-type GATA1 (Figure 5D and supplemental figure 8).

Discussion

In this study, we assessed two pedigrees displaying a variant in the *GATA1* gene. We report the first description of a variant in the C-terminal ZF of GATA1 that initially manifested as mucocutaneous bleeding with platelet dysfunction but without thrombocytopenia, which appeared later in life. We observed increased MYH10 levels in platelets, thus highlighting the persistence of MYH10 expression during MK differentiation, which may explain the decrease in MK ploidy and reduced platelet formation. Assessing published ChIP-sequence data and using reporter cell and mutagenesis assays, we demonstrated that GATA1 repressed *MYH10* expression via intronic binding sites in the *MYH10* gene.

To date, nearly all reported GATA1 variants have been shown to involve the N-terminal ZF (positions 205, 208, 216 and 218) and the intron/exon boundaries of exon 2 [22]; with the exception of the terminal p.X414R variant, which cause removal of the terminal codon and adds 42 extra amino acids to the full-length GATA1 protein [23]. Variants in the N-terminal ZF and at position 414 are associated with thrombocytopenia, while variants in exon 2 essentially lead to changes in the red blood cell lineage, leading to severe anemia or Diamond-Blackfan anemia. Currently, variants in the C-terminal ZF have not been described. The p.H289R variant, localized immediately 3' of the C-terminal ZF, has been reported to be not as damaging as variants affecting the N-terminal ZF domain [24].

In this study, we describe two novel *GATA1* variants. The patient harboring the variant at position 206 suffered from moderate bleeding with severe thrombocytopenia and mild dyserythropoietic features.

This observation agrees with previous descriptions of N-terminal ZF variants. Accordingly, this variation impairs FOG1 binding. The second variant identified affected the C-terminal ZF. Unlike variations in the N-terminal ZF, the p.L268M variation does not affect the GATA1/FOG1 interaction. The clinical characteristics resemble those observed with the p.R216Q variant localized in the DNA-binding surface of the N-terminal ZF, including macrothrombocytopenia, red blood cell abnormalities and minor beta-thalassemia [25–28]. Presentation was also close to the one described for the H289R variation. As in the F2 patients, the hemizygous males harbouring the H289R substitution exhibit increased MCV but normal hemoglobin levels. Thrombocytopenia was present only in two of the four affected family members [24]. Although both F2 children presented with high level of fetal hemoglobin, the absence of thrombocytopenia did not initially direct towards a GATA1 related disease. Indeed, the disease initially manifested as severe mucocutaneous bleeding associated with reduced platelet aggregation without thrombocytopenia. Platelet exploration carried out on several occasions did not make it possible to link the platelet phenotype to a known thrombopathy. Indeed, GPIIbIIIa was expressed at a normal level and was able to bind PAC1 antibody after activation by 10µM ADP. No sign of immune deficiency was observed in these children excluding a kindlin 3 deficiency [29]. Finally, the results of platelet aggregation were not in favor of a CalDAG-GEFI deficiency as platelet activation induced by a high concentration of arachidonic acid, identical to the one used in this article usually gives normal results [30]. For a long time, these children were considered to be carriers of a storage pool disease because of the early detection of a severe deficit of dense granules. These results are to be connected with those of White *et al* [31] who observed a near absence of dense bodies in the platelets from a patient with the R216Q GATA1 mutation. Although rescue experiments have not be performed and causality has not been shown, our results support the idea that the spectrum of *GATA1*-related diseases may be extended to include X-linked bleeding diathesis without thrombocytopenia, associated with collagen and arachidonic acid aggregation defects. In contrast to studies in Gata1-deficient mice [9,11,27,32] we did not observe reduced protein levels of GPVI, SYK or other key molecules involved in collagen signaling pathways, such as PLCγ2 that could explain the aggregation defect. The decrease in TBXAS1 levels observed in the two F2 brothers may play a

role in the reduced response to arachidonic acid. However, the platelets also failed to respond to U46619, thus indicating a more complex mechanism. The granule deficiency observed in the current study may also contribute to the platelet aggregation defects, although a complete lack of arachidonic acid- or collagen-induced platelet aggregation is not a feature of granule deficiency. Overall, further studies are required to understand the cause of platelet dysfunction observed in *GATA1* variant carriers. Thrombocytopenia developed gradually over time associated with an enlargement in red blood cells, indicating progression of the disease in p.L268M carriers. Cell-type-specific gene regulation may change during ontogeny. There are substantial developmental differences between neonates and adults in the process of megakaryopoiesis and in their responses to TPO [33]. Wenqing and colleagues have highlighted fundamental and conserved differences at distinct developmental stages, characterized by simpler promoter-centric regulation of cell-type-specific genes in embryonic cells and increased combinatorial enhancer-driven control in adult cells [34]. Overall, the delayed onset of thrombocytopenia observed in the F2 family suggest developmental stage-specific GATA-1 regulation.

Assessment of MKs in *GATA1* variant carriers revealed polyploidization and differentiation defects. Assessment of the p.N206I variant revealed a marked decrease in mature $CD41^{high}CD42a^{high}$ MKs, along with an increase in $CD41^{-}CD42a^{-}$ cells. Although we cannot formally exclude impaired expression of CD41 and CD42a in MKs harboring a GATA1 variant, the reduction in high-ploidy cells confirmed the MK maturation defect.

Additionally, the GATA1 N206I carrier displayed an increase in circulating CD34+ progenitor cells, as described for individuals carrying a germline ETV6 variants [27]. Recently, Shin *et al.* [36] have found that Gata1 low megakaryocyte-erythroid progenitors/megakaryocyte precursors cell lines display accelerated replication after approximately 90–100 days of culture. The observed increase in CD34+ cells may reflect this high proliferative capacity.

The polyploidization defect associated with GATA1 is not well understood. MYH10 has been shown to be required for cytokinesis during meiotic cell division [37] and to contribute to MK polyploidisation [13,38]. RUNX1-mediated silencing of *MYH10* has been found to be required for MK polyploidization

and may serve as a biomarker of *RUNX1* variants in patients [15]. FLI1 forms a complex with RUNX1 to regulate megakaryopoiesis. Carriers of *FLI1* variants also exhibit elevated MYH10 levels in platelets [15–17]. Interestingly, using a genome-wide analysis of simultaneous transcription factor binding in human MKs and ENCODE ChIP-sequence data, we have shown that FLI1, RUNX1 and GATA1 accumulate at regulatory elements in intron 8 and the 3'UTR of the *MYH10* gene [19]. Additionally, these transcription factors cooperate during megakaryopoiesis as components of a large transcriptional complex [21,39], thereby suggesting that GATA1 may regulate MYH10 expression in cooperation with RUNX1 and FLI1. To our knowledge, *MYH10* has not yet been described as a target gene of GATA1. We observed abnormal persistence of MYH10 protein in the platelets of the three *GATA1* variant carriers. The mother of the two F2 brothers also exhibited a slight increase in MYH10 levels. In a reporter luciferase assay using the HEL cell line, both regulatory elements in intron 8 and the 3'UTR of *MYH10* were found be functional by inducing reduced transcriptional activity. Disruption of the four intronic binding sites fully reversed the repressive activity, thus indicating that the intronic binding sites are required for *MYH10* repression, despite the presence of the other repressive complex partners (i.e., RUNX1, FLI1). The 3'UTR region of *MYH10* may preferentially bind to a portion of a protein complex that includes GATA1, without binding directly to GATA1. While GATA1 wild-type enhanced luciferase activity via the MYH10 intronic region in MSR cells, the opposite effect was observed in HEL cells. GATA1 is known to have both activating and repressing activity depending on the cellular and promoter/enhancer context [40]. Variations in the expression of GATA1 partners in these two cell models, such as RUNX1 and FLI1, may explain these differences. In MSR cells, the GATA1 responsive activity decreased in presence of each variant, compared with wild-type *GATA1*, indicating that the increase in MYH10 levels observed in patients likely results from reduced interaction between the product of the *GATA1* variants and the *MYH10* intronic region. Intronic GATA1 binding sites have already been shown to be involved in the regulation of 5-aminolevulinate synthase 2 (*ALAS2*) gene expression, which is involved in heme synthesis in erythroid cells [41].

In summary, we describe two novel pathogenic variations in the *GATA1* gene characterized by distinct clinical and laboratory findings. Our results suggest that variants affecting the GATA1 C-terminal ZF

should likely be assessed in patients with normal platelet counts and platelet aggregation defects in response to collagen and arachidonic. Importantly, Both GATA1 variants analyzed in this study led to persistent expression of MYH10 in platelets. We identify a *MYH10* intronic region that functions as a GATA1-responsive cis-regulatory element.

Acknowledgments

The study was funded by the “Fondation pour la Recherche Médicale” (granted to PS: FDM20150633607), the French Foundation for Rare Diseases (grant WES 2012-2001), the National Institutes of Diabetes, Digestive and Kidney diseases (NIDDK) of the National Institutes of Health (granted to JVA: DK101628). The authors acknowledge the members of the French Reference Center for Inherited Hereditary Platelet Disorders (CRPP) for their contribution to clinical analysis of the patients and Dr. M Fiore for providing patient samples.

Author contributions

PS, SA, and MaP designed and performed the experiments, analyzed the data and wrote the manuscript. DP, DPB, MiP, FP and MC analyzed the data and revised the manuscript. NS performed DNA sequencing and revised the manuscript. JCB performed TEM analysis and revised the manuscript. JvA performed the structure analysis experiments and revised the manuscript. DB, ML, CF and PEM performed clinical and biological characterization of patients, analyzed the data and revised the manuscript. MP and MCA supervised the study and wrote the manuscript.

Declaration of interest

The authors have declared that no conflict of interest exists.

References

1 Crispino JD. GATA1 in normal and malignant hematopoiesis. *Semin Cell Dev Biol* 2005; **16**: 137–47.

2 Crispino JD, Horwitz MS. GATA factor mutations in hematologic disease. *Blood* 2017; **129**: 2103–10.

3 Songdej N, Rao AK. Hematopoietic transcription factor mutations: important players in inherited platelet defects. *Blood* 2017; **129**: 2873–81.

4 Ko LJ, Engel JD. DNA-binding specificities of the GATA transcription factor family. *Mol Cell Biol* 1993; **13**: 4011–22.

5 Mehaffey MG, Newton AL, Gandhi MJ, Crossley M, Drachman JG. X-linked thrombocytopenia caused by a novel mutation of GATA-1. *Blood* 2001; **98**: 2681–8.

6 Nichols KE, Crispino JD, Poncz M, White JG, Orkin SH, Maris JM, Weiss MJ. Familial dyserythropoietic anaemia and thrombocytopenia due to an inherited mutation in GATA1. *Nat Genet* 2000; **24**: 266–70.

7 Chang AN, Cantor AB, Fujiwara Y, Lodish MB, Droho S, Crispino JD, Orkin SH. GATA-factor dependence of the multitype zinc-finger protein FOG-1 for its essential role in megakaryopoiesis. *PNAS* National Academy of Sciences; 2002; **99**: 9237–42.

8 Shivdasani RA, Fujiwara Y, McDevitt MA, Orkin SH. A lineage-selective knockout establishes the critical role of transcription factor GATA-1 in megakaryocyte growth and platelet development. *EMBO J* 1997; **16**: 3965–73.

9 Vyas P, Ault K, Jackson CW, Orkin SH, Shivdasani RA. Consequences of GATA-1 deficiency in megakaryocytes and platelets. *Blood* 1999; **93**: 2867–75.

10 Muntean AG, Pang L, Poncz M, Dowdy SF, Blobel GA, Crispino JD. Cyclin D-Cdk4 is regulated by GATA-1 and required for megakaryocyte growth and polyploidization. *Blood* 2007; **109**: 5199–207.

11 Meinders M, Hoogenboezem M, Scheenstra MR, De Cuyper IM, Papadopoulos P, Németh T, Mócsai A, van den Berg TK, Kuijpers TW, Gutiérrez L. Repercussion of Megakaryocyte-Specific Gata1 Loss on Megakaryopoiesis and the Hematopoietic Precursor Compartment. *PLoS ONE* 2016; **11**: e0154342.

12 Mazzi S, Lordier L, Debili N, Raslova H, Vainchenker W. Megakaryocyte and polyploidization. *Exp Hematol* 2018; **57**: 1–13.

13 Lordier L, Bluteau D, Jalil A, Legrand C, Pan J, Rameau P, Jouni D, Bluteau O, Mercher T, Leon C, Gachet C, Debili N, Vainchenker W, Raslova H, Chang Y. RUNX1-induced silencing of non-muscle myosin heavy chain IIB contributes to megakaryocyte polyploidization. *Nat Commun* 2012; **3**: 717.

14 Bluteau D, Glembotsky AC, Raimbault A, Balayn N, Gilles L, Rameau P, Nurden P, Alessi MC, Debili N, Vainchenker W, Heller PG, Favier R, Raslova H. Dysmegakaryopoiesis of FPD/AML pedigrees with constitutional RUNX1 mutations is linked to myosin II deregulated expression. *Blood* 2012; **120**: 2708–18.

15 Antony-Debré I, Bluteau D, Itzykson R, Baccini V, Renneville A, Boehlen F, Morabito M, Droin N, Deswarte C, Chang Y, Leverger G, Solary E, Vainchenker W, Favier R, Raslova H. MYH10 protein expression in platelets as a biomarker of RUNX1 and FLI1 alterations. *Blood* 2012; **120**: 2719–22.

16 Stockley J, Morgan NV, Bem D, Lowe GC, Lordkipanidzé M, Dawood B, Simpson MA, Macfarlane K, Horner K, Leo VC, Talks K, Motwani J, Wilde JT, Collins PW, Makris M, Watson SP, Daly ME, UK Genotyping and Phenotyping of Platelets Study Group. Enrichment of FLI1 and RUNX1 mutations in families with excessive bleeding and platelet dense granule secretion defects. *Blood* 2013; **122**: 4090–3.

17 Stevenson WS, Rabbolini DJ, Beutler L, Chen Q, Gabrielli S, Mackay JP, Brighton TA, Ward CM, Morel-Kopp M-C. Paris-Trousseau thrombocytopenia is phenocopied by the autosomal recessive inheritance of a DNA-binding domain mutation in FLI1. *Blood* 2015; **126**: 2027–30.

18 Saultier P, Vidal L, Canault M, Bernot D, Falaise C, Pouymayou C, Bordet J-C, Saut N, Rostan A, Baccini V, Peiretti F, Favier M, Lucca P, Deleuze J-F, Olaso R, Boland A, Morange PE, Gachet C, Malergue F, Fauré S, et al. Macrothrombocytopenia and dense granule deficiency associated with FLI1 variants: ultrastructural and pathogenic features. *Haematologica* 2017; **102**: 1006–16.

19 Tijssen MR, Cvejic A, Joshi A, Hannah RL, Ferreira R, Forrai A, Bellissimo DC, Oram SH, Smethurst PA, Wilson NK, Wang X, Ottersbach K, Stemple DL, Green AR, Ouwehand WH, Göttgens B. Genome-wide analysis of simultaneous GATA1/2, RUNX1, FLI1, and SCL binding in megakaryocytes identifies hematopoietic regulators. *Dev Cell* 2011; **20**: 597–609.

20 Xu G, Kanezaki R, Toki T, Watanabe S, Takahashi Y, Terui K, Kitabayashi I, Ito E. Physical association of the patient-specific GATA1 mutants with RUNX1 in acute megakaryoblastic leukemia accompanying Down syndrome. *Leukemia* 2006; **20**: 1002–8.

21 Elagib KE, Racke FK, Mogass M, Khetawat R, Delehanty LL, Goldfarb AN. RUNX1 and GATA-1 coexpression and cooperation in megakaryocytic differentiation. *Blood* 2003; **101**: 4333–41.

22 Kobayashi E, Shimizu R, Kikuchi Y, Takahashi S, Yamamoto M. Loss of the Gata1 gene IE exon leads to variant transcript expression and the production of a GATA1 protein lacking the N-terminal domain. *J Biol Chem* 2010; **285**: 773–83.

23 Singleton BK, Roxby DJ, Stirling JW, Spring FA, Wilson C, Poole J, Anstee DJ. A novel GATA1 mutation (Stop414Arg) in a family with the rare X-linked blood group Lu(a-b-) phenotype and mild macrothrombocytic thrombocytopenia. *Br J Haematol* 2013; **161**: 139–42.

24 Pereira J, Bento C, Manco L, Gonzalez A, Vagace J, Ribeiro ML. Congenital dyserythropoietic anemia associated to a GATA1 mutation aggravated by pyruvate kinase deficiency. *Ann Hematol* 2016; **95**: 1551–3.

25 Yu C, Niakan KK, Matsushita M, Stamatoyannopoulos G, Orkin SH, Raskind WH. X-linked thrombocytopenia with thalassemia from a mutation in the amino finger of GATA-1 affecting DNA binding rather than FOG-1 interaction. *Blood* 2002; **100**: 2040–5.

26 Balduini CL, Pecci A, Loffredo G, Izzo P, Noris P, Grosso M, Bergamaschi G, Rosti V, Magrini U, Ceresa IF, Conti V, Poggi V, Savoia A. Effects of the R216Q mutation of GATA-1 on erythropoiesis and megakaryocytopoiesis. *Thromb Haemost* 2004; **91**: 129–40.

27 Hughan SC, Senis Y, Best D, Thomas A, Frampton J, Vyas P, Watson SP. Selective impairment of platelet activation to collagen in the absence of GATA1. *Blood* 2005; **105**: 4369–76.

28 Åström M, Hahn-Strömberg V, Zetterberg E, Vedin I, Merup M, Palmblad J. X-linked thrombocytopenia with thalassemia displays bone marrow reticulin fibrosis and enhanced angiogenesis: comparisons with primary myelofibrosis. *Am J Hematol* 2015; **90**: E44-48.

29 Robert P, Canault M, Farnarier C, Nurden A, Grosdidier C, Barlogis V, Bongrand P, Pierres A, Chambost H, Alessi M-C. A novel leukocyte adhesion deficiency III variant: kindlin-3 deficiency results in integrin- and nonintegrin-related defects in different steps of leukocyte adhesion. *J Immunol* 2011; **186**: 5273–83.

30 Canault M, Ghalloussi D, Grosdidier C, Guinier M, Perret C, Chelghoum N, Germain M, Raslova H, Peiretti F, Morange PE, Saut N, Pillois X, Nurden AT, Cambien F, Pierres A, van den Berg TK, Kuijpers TW, Alessi M-C, Tregouet D-A. Human CalDAG-GEFI gene (RASGRP2) mutation affects platelet function and causes severe bleeding. *J Exp Med* 2014; **211**: 1349–62.

31 White JG, Thomas A. Platelet structural pathology in a patient with the X-linked GATA-1, R216Q mutation. *Platelets* 2009; **20**: 41–9.

32 Ferreira R, Ohneda K, Yamamoto M, Philipsen S. GATA1 function, a paradigm for transcription factors in hematopoiesis. *Mol Cell Biol* 2005; **25**: 1215–27.

33 Liu Z-J, Italiano J Jr, Ferrer-Marin F, Gutti R, Bailey M, Poterjoy B, Rimsza L, Sola-Visner M. Developmental differences in megakaryocytopoiesis are associated with up-regulated TPO signaling through mTOR and elevated GATA-1 levels in neonatal megakaryocytes. *Blood* 2011; **117**: 4106–17.

34 Cai W, Huang J, Zhu Q, Li BE, Seruggia D, Zhou P, Nguyen M, Fujiwara Y, Xie H, Yang Z, Hong D, Ren P, Xu J, Pu WT, Yuan G-C, Orkin SH. Enhancer dependence of cell-type-specific gene expression increases with developmental age. *Proc Natl Acad Sci U S A* 2020; **117**: 21450–8.

35 Poggi M, Canault M, Favier M, Turro E, Saultier P, Ghalloussi D, Baccini V, Vidal L, Mezzapesa A, Chelghoum N, Mohand-Oumoussa B, Falaise C, Favier R, Ouwehand WH, Fiore M, Peiretti F, Morange PE, Saut N, Bernot D, Greinacher A, et al. Germline variants in ETV6 underlie reduced platelet formation, platelet dysfunction and increased levels of circulating CD34+ progenitors. *Haematologica* 2017; **102**: 282–94.

36 Shin E, Jeong J-G, Chung H, Jung H, Park C, Yoon SR, Kim T-D, Lee SJ, Choi I, Noh J-Y. The Gata1low murine megakaryocyte-erythroid progenitor cells expand robustly and alter differentiation potential. *Biochem Biophys Res Commun* 2020; **528**: 46–53.

37 Yang F, Wei Q, Adelstein RS, Wang PJ. Non-muscle myosin IIB is essential for cytokinesis during male meiotic cell divisions. *Dev Biol* 2012; **369**: 356–61.

38 Badirou I, Pan J, Legrand C, Wang A, Lordier L, Boukour S, Roy A, Vainchenker W, Chang Y. Carboxyl-terminal-dependent recruitment of nonmuscle myosin II to megakaryocyte contractile ring during polyploidization. *Blood* 2014; **124**: 2564–8.

39 Eisbacher M, Holmes ML, Newton A, Hogg PJ, Khachigian LM, Crossley M, Chong BH. Protein-protein interaction between Fli-1 and GATA-1 mediates synergistic expression of megakaryocyte-specific genes through cooperative DNA binding. *Mol Cell Biol* 2003; **23**: 3427–41.

40 Welch JJ, Watts JA, Vakoc CR, Yao Y, Wang H, Hardison RC, Blobel GA, Chodosh LA, Weiss MJ. Global regulation of erythroid gene expression by transcription factor GATA-1. *Blood* 2004; **104**: 3136–47.

41 Zhang Y, Zhang J, An W, Wan Y, Ma S, Yin J, Li X, Gao J, Yuan W, Guo Y, Engel JD, Shi L, Cheng T, Zhu X. Intron 1 GATA site enhances ALAS2 expression indispensably during erythroid differentiation. *Nucleic Acids Res* 2017; **45**: 657–71.

Figure legend

Figure 1. Identification of two novel GATA1 variants.
A) Pedigrees of the affected families. Squares denote males, and circles represent females. The slashes denote deceased family members. Solid black symbols represent affected family members carrying a hemizygous *GATA1* variant. Circles with a dot represent heterozygous female carriers of the variants. Solid gray symbols represent non-tested family members with a medical history of bleeding events.
(B) Sanger sequencing electropherograms of the indicated family members.
(C) Schematic diagram of the GATA1 protein domain structure. The functional N-terminal transactivation domain (TD) and both the N- and C-terminal zinc-finger domains (ZF1 and ZF2, respectively) are depicted. The positions of the variations within GATA1 are indicated in red (variations reported in this study) and black (variations reported in previous studies).

(D) Left: Figure. Structure of Zn fingers of GATA1 bound to palindromic DNA recognition site (PDB code: 3VD6). The diagram shows GATA1 in green cartoon with key residues L268 and N206 in yellow sticks, and the DNA fragment in magenta sticks. Zn2+ ions are in grey spheres with stick representation of coordinating residues. Other GATA1 relevant variants V205M and G208R are mapped in orange sticks. Inset A show 3VD6 superimposed to the same structure harboring a model of the L268M mutation. Right: Lowest energy conformer of NMR structure of Zn fingers of GATA1 bound to FOG1 (PDB code: 1Y0J). The diagram shows GATA1 in green cartoon with key residue N206 in yellow stick, and FOG1 in red. Zn2+ ions are in grey spheres with stick representation of coordinating residues. Other GATA1 relevant variants V205M and G208R are mapped in orange sticks. Inset A shows 1Y0J superimposed to the same structure harboring a model of the N206I mutation. In dashes is shown an atomic clash between I206 (GATA1) and Y30 (FOG1) with interatomic distances below 2.5 Å.

Figure 2. Quantitative and morphological modifications of platelets and red blood cells in GATA1 variant carriers

(A) Evolution of platelet count and mean corpuscular volume (MCV) of erythrocytes with age in the two F2 probands.

(B) **Representative images of peripheral blood smears** stained with May-Grünwald-Giemsa for patients F1-II-1 and F2-II-2 (at 6 and 23 years old, respectively). The peripheral blood smear images revealed hypogranular platelets (left, black arrow, magnification x1000) mild anisocytosis and poikylocytosis (right, magnification x 500).

(C) **Representative images of bone marrow aspirate smears** stained with May-Grünwald-Giemsa for patient F1-II-1 (at 17 months old). Assessment of bone marrow aspirates revealed dysmegakaryopoiesis with hypolobulated megakaryocytes (left, black arrow, magnification x 200) and dyserythropoiesis with nuclear karyorrhexis (right, black arrow, magnification x500). Smears were examined for each subject by a well-trained hematologist (M Loosveld).

Figure 3. Alpha and dense granule defects associated with GATA1 variants.

(A) Representative micrographs of dense granule distribution in a control and patients F1-II-1 (at 8 years old), F2-II-1 (at 27 years old) and F2-II-2 (at 23 years old). Scale bar: 1 µm. The graph shows the cumulative distribution of dense granules per whole platelet deposited on formar film for patient vs. control platelets (healthy subjects, n=54); 100 platelets per whole-platelet mount were examined for each subject by a well-trained engineer blinded to the genotype (JC Bordet, Unité d'Hémostase Biologique, Bron, France).

(B) Platelet sections from a healthy subject (control panel) and patient F2-II-1 (all other panels). Platelet section from control shows numerous alpha granules, mitochondria recognizable by the crests, and a large glycogen area. Although the numbers are variable, platelets derived from patient F2-II-1 at 22 years old displayed low alpha granule counts for each section, sometimes lower than mitochondria counts. Overall, the sections display either very few organelles with a relatively amorphous background (i) or normal counts for organelles that show variable granulation (iv). Other notable structures observed included very large areas of membrane complexes (ii, iii) and apoptotic granules (left part of panel iii). We also observed membranous formations that resemble a dense tubular system, although the formations were occasionally arranged in a large ring (i), in the vicinity of the tubulin circle (bottom center panel) or in aggregates in the cytoplasm (v). Scale bar: 0.5 µm. The graphs show the cumulative distribution of platelet area, number of alpha granules/µm^2, major platelet diameter, and alpha granule diameter using classical electron microscopy sections in patient F2-II-1 vs. control platelets (healthy subjects n=10); we examined 100 platelets per section.

Figure 4. Increased number of CD34$^+$ cells and abnormal megakaryocyte differentiation in GATA1 variant carriers.

(A) Flow cytometry analysis of circulating CD34$^+$ cells. Left: Representative dot plots of cells from one healthy control and patient F1-II-1. The plots display the side scatter and CD34 expression analysis in CD19low CD45low cells. The ellipse gates show the CD19low CD45low CD34+ cell population. Right: The percentage of CD34$^+$ cells in the total CD19low CD45low cell population. The control data

represent five different individuals. The data for patient F1-II-1 was obtained from two independent experiments carried out at 15-month intervals. The data are provided as the median ± interquartile range.
(B-D) In vitro megakaryocyte differentiation. Circulating $CD34^+$ cells from F1-II-1 patient or controls were isolated and cultured in the presence of TPO and SCF to induce megakaryocytic commitment. **(B)** Megakaryocyte differentiation was monitored via flow cytometry. The density plots display the CD41/CD42a expression profiles of two unrelated controls and F1-II-1 affected patient (at days 9 and 11 of differentiation**)**. **(C)** Representative images of cultured cells at day 11 (20X magnification). The graph represents the median ± interquartile range of the cell surface area. Fifty cells were quantified. Differences between the groups were assessed using the Kruskal-Wallis test followed by Dunn's multiple comparison test. **(D)** Ploidy levels were monitored via flow cytometry. The histograms display the frequency distribution of Hoechst 33342 levels in $CD34^+$-derived cells from two unrelated controls and F1-II-1 affected patient at day 9 of differentiation.
(E) Western blot analysis of MYH10 expression in platelets from the patients with GATA1 variants (F1-II2, F2-II-1 and F2-II-2), one heterozygous carrier (F2-I-1), one unaffected family member (F2-I-2) and four unrelated controls. Platelets from a patient carrying the FLI1 p R337Q variant represents the MYH10 positive control. GAPDH was used as a protein loading control. Quantification of band intensity for MYH10 is shown below the western blot.

Figure 5. Identification and functional analysis of the MYH10 regulatory regions.
(A) Visualization of *MYH10* regulatory regions with GATA1, FLI1 and RUNX1 binding peaks identified via ChIP-sequencing. Part of the *NDEL* gene is shown upstream of the *MYH10* gene using the UCSC genome browser (chr17:8,435,074-8,669,900 using GRCh38/hg38). The bottom layer shows the position of two GATA1 binding region peaks within the 3'UTR (untranslated transcribed region, blue arrows) and intron 8 (red arrows) of *MYH10* for the transcription factors GATA1, FLI1 and RUNX1.
(B) Luciferase expression in HEL cells transfected with different pGL3 luciferase reporter vectors including the 3'UTR or intron 8 regions of *MYH10* gene. Mutations on GATA1-binding sites in intron 8 were introduced as indicated (M1 or M2 or M3 or M(1,2,3,4)). The pGL3 vector without regulatory regions (empty vector) was used as a control. Each plasmid was assayed in three to seven independent transfection experiments. The dual luciferase assay was performed by sequentially measuring the firefly and renilla luciferase activities of the same sample with the results expressed as the ratio of firefly to renilla activity (Fluc/Rluc). **: $p<0.001$, ***: $p<0.0001$ vs. pGL3-intron 8 MYH10 wild-type (WT) (one-way ANOVA corrected for multiple comparisons). +++: $p<0.0001$ vs. pGL3-empty vector (one-way ANOVA corrected for multiple comparisons).
(C) Luciferase expression in GripTite 293 MSR cells transfected with different pGL3 luciferase reporters and pCDNA3-GATA1 vectors as indicated. Left: pGL3-intron 8 MYH10 wild-type (WT), pGL3-intron 8 MYH10 mutants, empty pCDNA3 and pCDNA3-GATA1 WT. Middle: pGL3-3'UTR MYH10, empty pCDNA3 and pCDNA3-GATA1 WT. Right: empty pGL3, empty pCDNA and pCDNA-GATA1 WT. The pCDNA3 empty vector was used as a control. *: $p<0.01$, ****: $p<0.0001$ vs. pGL3-intron8-MYH10 WT in the presence of GATA1 (black bar) (one-way ANOVA corrected for multiple comparisons). ++++: $p<0.0001$ vs. the empty pGL3 vector in the absence of GATA1 (white bar). Each plasmid was assayed in six separate transfection experiments (one-way ANOVA corrected for multiple comparisons).
(D) Luciferase expression after transfection in GripTite 293 MSR cells with pGL3-intron 8 MYH10 WT and pCDNA3-GATA1 WT or variant vectors as indicated. *: $p<0.01$ vs. GATA1 WT (one-way ANOVA corrected for multiple comparisons). Each plasmid was assayed in five separate transfection experiments.

Table 1. Platelet aggregation assays

Results correspond to assays performed in 1990 and 1993 (A) and 2015 (B).

A

Individuals	Age (years)	Blood platelet count (x 10^9/l)	PRP platelet count (x 10^9/l)	Platelet aggregation maximal intensity (%)					
				ADP		Collagen		Arachidonic acid	Ristocetine
				1 µM	2.5 µM	0.36 µg/ml	0.72 µg/ml	0.5 mg/ml	1.5 mg/ml
Control *	NA	NA	350	45	68	60	63	69	76
F2-II-1	1.7	233	380	9	25	0	0	19	67
Control *	NA	NA	350	45	68	57	63	69	68
F2-II-2	0.8	225	338	8	23	0	0	11	46

B

Individuals	Age (years)	Blood platelet count (x 10^9/l)	PRP platelet count (x 10^9/l)	Platelet aggregation maximal intensity (%)					
				ADP			Collagen	Arachidonic acid	Ristocetine
				2.5 µM	5 µM	10 µM	3.3 µg/ml	0.5 mg/ml	1.25 mg/ml
Normal range				83-93	75-90	78-92	79-85	76-91	78-948
F2II-1	26.7	106	159	40	62	56	25	14	73
F2II-2	22.7	58	102	40	62	68	24	11	70

* Controls correspond to one healthy individual tested at the same time.

Table 2. Platelet glycoprotein expression

Platelet glycoprotein MFI (a.u.)		Individuals				
		F1-II-1	Normal range *(10^{th}-90^{th} range n = 14)*	F2-II-1	F2-II-2	Normal range *(10^{th}-90^{th} range n = 12)*
αIIbβ3 (CD41)	Basal	24	21-44	24	30	20-29
	TRAP14 50µM	25	30-62	30	34	28-46
GPIbα (CD42b)	Basal	1.7	1.2-.3	2.1	2.4	1.2-2.4
	TRAP14 50µM	1.5	0.9-2.3	1.8	1.8	0.6-1.1
CD63	Basal	1.2	0.9-3.4	1.1	1.3	0.5-1
	TRAP14 50µM	1.6	1.9-6.3	1.7	1.3	1.3-3.6
	Ratio TRAP-14 / basal	1.3	1.7-3.7	1.4	1	1.5-4.8
CD62P (P-selectin)	Basal	0.2	0.09-0.35	0.2	0.4	0.15-0.75
	TRAP14 50µM	0.2	1.9-6.3	1.5	1.7	2.3-5
	Ratio TRAP-14 / basal	1.1	12.4-22.8	7	4.2	5.5-25

Table 3. Characteristics of GATA1 variant carriers

	Family 1 (F1-II-1)	Family 2 (F2-II-1 and F2-II-2)
DNA change	c.802C>A	C617A>T
Protein change	p.N206I	p.L268M
Variant localization	N-terminal zinc finger	C-terminal zinc finger
Clinical manifestations		
Thrombocytopenia	Early in life (18 months) with a severely reduced platelet count (15 G/L).	Initially absent (at 18 and 9 months, 261 and 233 G/L for each brother). Thrombocytopenia gradually developed from 2-5 years of age and then steadily worsened.
Bleeding	Frequent bruising, post vaccinal hematoma.	Pronounced mucocutaneous bleedings.
	Bleeding during dental avulsion prevented by platelet concentrates.	Bleeding during dental avulsion and appendicectomy was prevented by platelet concentrates.
Platelet	Not done	Bleeding time >15min
	No aggregation test performed (because platelet number is < 20G/L).	Aggregation defect (mainly collagen and arachidonic acid) in absence of thrombocytopenia.
	> 90% reduction in dense granule number.	≥ 90% reduction in dense granule number for both children.
	Surface glycoproteins: No basal defect in CD41, CD42b, CD62P, and CD63; reduced expression levels of CD63 and CD62P after TRAP-14 stimulation.	Surface glycoproteins: No basal defect in CD41, CD42b, CD62P, and CD63; reduced expression levels of CD63 and CD62P after TRAP-14 stimulation.
	Serotonin: NA (too low platelet count).	Serotonin low values in both children: 0.12-0.16 µg/10^9 platelets (Normal values: 0.3-1.20).
	PAI-1 antigen: normal value, 0.35 ng/10^6 platelets (Normal values: 0.33-1.07).	PAI-1 antigen: normal values in both child 0.69-0.76 ng/10^6 platelets (Normal values: 0.33-1.07).
Coagulation and fibrinolysis	No defect.	No defect.
Erythrocyte	Absence of anemia.	Absence of anemia.
	MCV : 77-81 fL (Normal values : 80-95).	Progressive increase in MCV over time (from 85-90 to 99 and 103 fL at 26 and 23 years of age) (Normal values: 80-95).
	Discrete anisopoïkilocytosis, few dacryocytes and schizocytes.	Anisopoikilocytosis.
	Fetal hemoglobin not evaluated.	Elevated level of fetal hemoglobin (25%).
Bone marrow	Dysmegakaryopoiesis with hypolobulated megakaryocytes and mild dyserythropoiesis with nuclear karyorrhexis.	Not done.

1

FIGURE 1

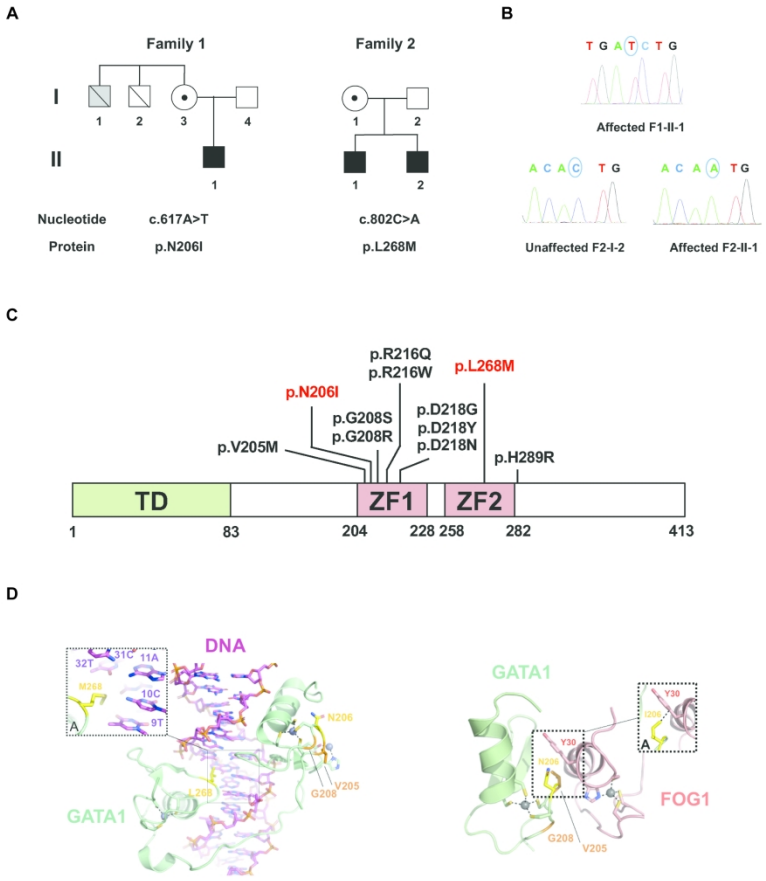

Figure 1. Identification of two novel GATA1 variants.
A) Pedigrees of the affected families. Squares denote males, and circles represent females. The slashes denote deceased family members. Solid black symbols represent affected family members carrying a hemizygous GATA1 variant. Circles with a dot represent heterozygous female carriers of the variants. Solid gray symbols represent non-tested family members with a medical history of bleeding events.
(B) Sanger sequencing electropherograms of the indicated family members.
(C) Schematic diagram of the GATA1 protein domain structure. The functional N-terminal transactivation domain (TD) and both the N- and C-terminal zinc-finger domains (ZF1 and ZF2, respectively) are depicted. The positions of the variations within GATA1 are indicated in red (variations reported in this study) and black (variations reported in previous studies).

209x296mm (300 x 300 DPI)

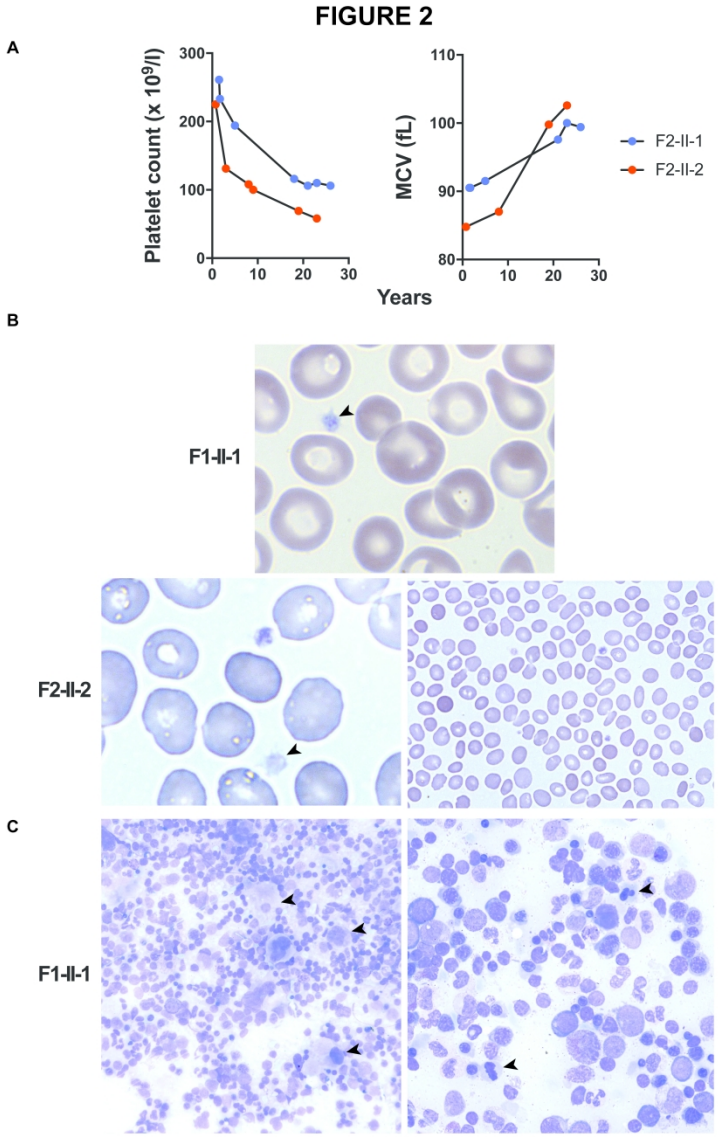

Figure 2. Quantitative and morphological modifications of platelets and red blood cells in GATA1 variant carriers

(A) Evolution of platelet count and mean corpuscular volume (MCV) of erythrocytes with age in the two F2 probands.(B) Representative images of peripheral blood smears stained with May-Grünwald-Giemsa for patients F1-II-1 and F2-II-2 (at 6 and 23 years old, respectively). The peripheral blood smear images revealed hypogranular platelets (left, black arrow, magnification x1000) mild anisocytosis and poikylocytosis (right, magnification x 500).(C) Representative images of bone marrow aspirate smears stained with May-Grünwald-Giemsa for patient F1-II-1 (at 17 months old). Assessment of bone marrow aspirates revealed dysmegakaryopoiesis with hypolobulated megakaryocytes (left, black arrow, magnification x 200) and dyserythropoiesis with nuclear karyorrhexis (right, black arrow, magnification x500). Smears were examined for each subject by a well-trained hematologist (M Loosveld).

FIGURE 3

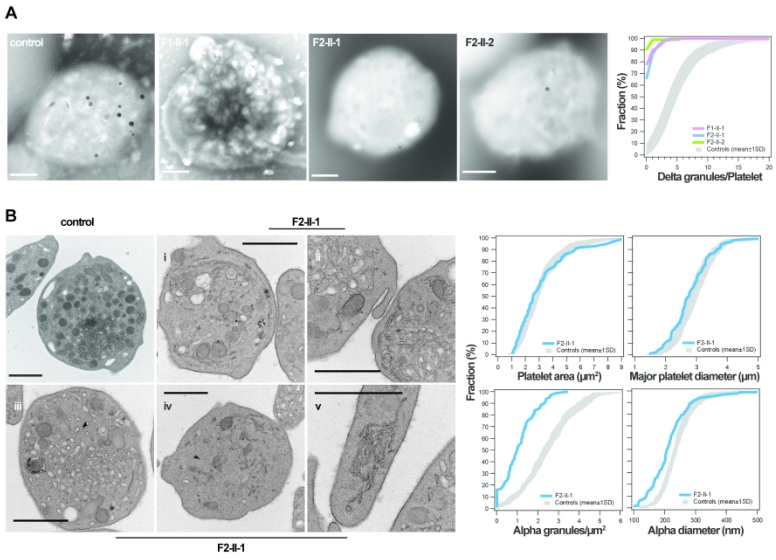

Figure 3. Alpha and dense granule defects associated with GATA1 variants.
(A) Representative micrographs of dense granule distribution in a control and patients F1-II-1 (at 8 years old), F2-II-1 (at 27 years old) and F2-II-2 (at 23 years old). Scale bar: 1 µm. The graph shows the cumulative distribution of dense granules per whole platelet deposited on formar film for patient vs. control platelets (healthy subjects, n=54); 100 platelets per whole-platelet mount were examined for each subject by a well-trained engineer blinded to the genotype (JC Bordet, Unité d'Hémostase Biologique, Bron, France). (B) Platelet sections from a healthy subject (control panel) and patient F2-II-1 (all other panels). Platelet section from control shows numerous alpha granules, mitochondria recognizable by the crests, and a large glycogen area. Although the numbers are variable, platelets derived from patient F2-II-1 at 22 years old displayed low alpha granule counts for each section, sometimes lower than mitochondria counts. Overall, the sections display either very few organelles with a relatively amorphous background (i) or normal counts for organelles that show variable granulation (iv). Other notable structures observed included very large areas of membrane complexes (ii, iii) and apoptotic granules (left part of panel iii). We also observed membranous formations that resemble a dense tubular system, although the formations were occasionally arranged in a

large ring (i), in the vicinity of the tubulin circle (bottom center panel) or in aggregates in the cytoplasm (v). Scale bar: 0.5 μm. The graphs show the cumulative distribution of platelet area, number of alpha granules/μm2, major platelet diameter, and alpha granule diameter using classical electron microscopy sections in patient F2-II-1 vs. control platelets (healthy subjects n=10); we examined 100 platelets per section.

FIGURE 4

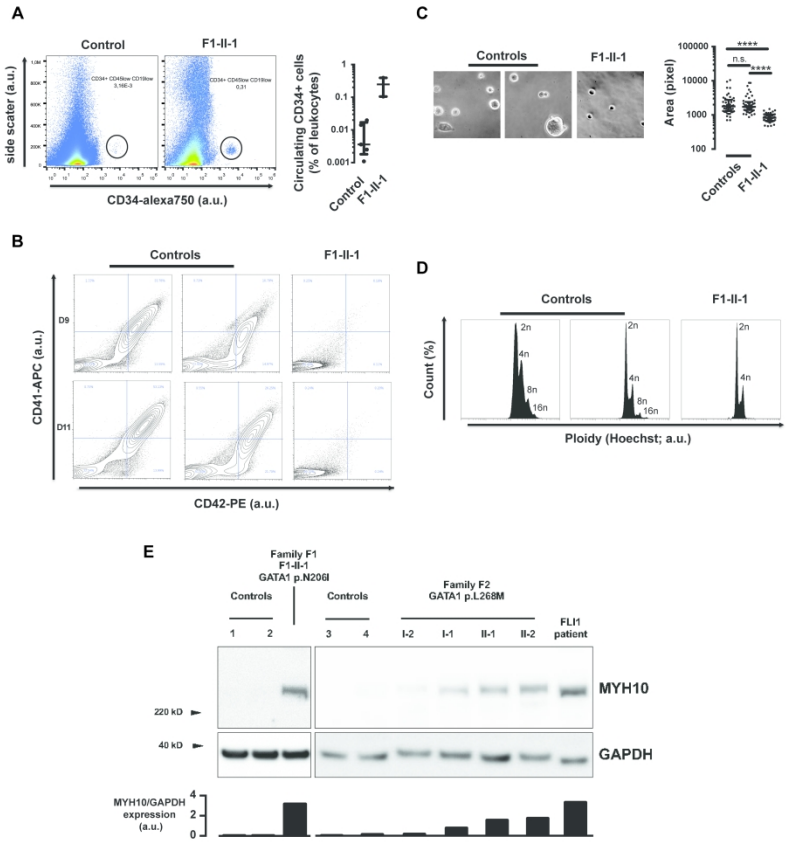

Figure 4. Increased number of CD34+ cells and abnormal megakaryocyte differentiation in GATA1 variant carriers.

(A) Flow cytometry analysis of circulating CD34+ cells. Left: Representative dot plots of cells from one healthy control and patient F1-II-1. The plots display the side scatter and CD34 expression analysis in CD19low CD45low cells. The ellipse gates show the CD19low CD45low CD34+ cell population. Right: The percentage of CD34+ cells in the total CD19low CD45low cell population. The control data represent five different individuals. The data for patient F1-II-1 was obtained from two independent experiments carried out at 15-month intervals. The data are provided as the median ± interquartile range.

(B-D) In vitro megakaryocyte differentiation. Circulating CD34+ cells from F1-II-1 patient or controls were isolated and cultured in the presence of TPO and SCF to induce megakaryocytic commitment. (B) Megakaryocyte differentiation was monitored via flow cytometry. The density plots display the CD41/CD42a expression profiles of two unrelated controls and F1-II-1 affected patient (at days 9 and 11 of differentiation). (C) Representative images of cultured cells at day 11 (20X magnification). The graph represents the median ± interquartile range of the cell surface area. Fifty cells were quantified. Differences

between the groups were assessed using the Kruskal-Wallis test followed by Dunn's multiple comparison test. (D) Ploidy levels were monitored via flow cytometry. The histograms display the frequency distribution of Hoechst 33342 levels in CD34+-derived cells from two unrelated controls and F1-II-1 affected patient at day 9 of differentiation.
(E) Western blot analysis of MYH10 expression in platelets from the patients with GATA1 variants (F1-II2, F2-II-1 and F2-II-2), one heterozygous carrier (F2-I-1), one unaffected family member (F2-I-2) and four unrelated controls. Platelets from a patient carrying the FLI1 p R337Q variant represents the MYH10 positive control. GAPDH was used as a protein loading control. Quantification of band intensity for MYH10 is shown below the western blot.

FIGURE 5

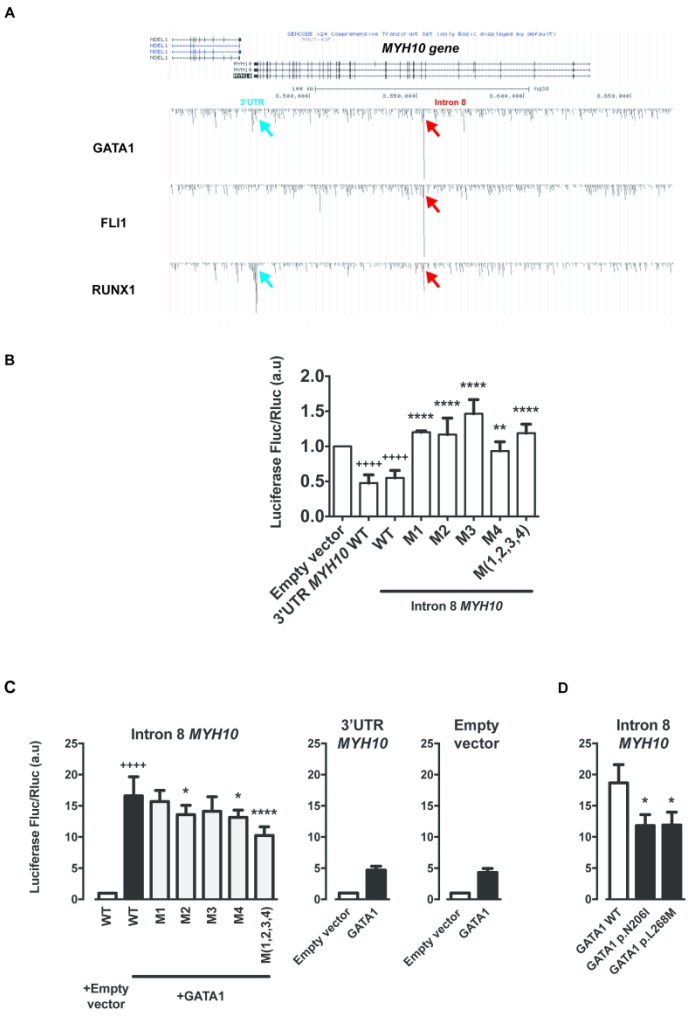

Figure 5. Identification and functional analysis of the MYH10 regulatory regions.
(A) Visualization of MYH10 regulatory regions with GATA1, FLI1 and RUNX1 binding peaks identified via ChIP-sequencing. Part of the NDEL gene is shown upstream of the MYH10 gene using the UCSC genome browser (chr17:8,435,074-8,669,900 using GRCh38/hg38). The bottom layer shows the position of two GATA1 binding region peaks within the 3'UTR (untranslated transcribed region, blue arrows) and intron 8 (red arrows) of MYH10 for the transcription factors GATA1, FLI1 and RUNX1.
(B) Luciferase expression in HEL cells transfected with different pGL3 luciferase reporter vectors including the 3'UTR or intron 8 regions of MYH10 gene. Mutations on GATA1-binding sites in intron 8 were introduced as indicated (M1 or M2 or M3 or M(1,2,3,4)). The pGL3 vector without regulatory regions (empty vector) was used as a control. Each plasmid was assayed in three to seven independent transfection experiments. The dual luciferase assay was performed by sequentially measuring the firefly and renilla luciferase activities of the same sample with the results expressed as the ratio of firefly to renilla activity (Fluc/Rluc). **: $p<0.001$, ***: $p<0.0001$ vs. pGL3-intron 8 MYH10 wild-type (WT) (one-way ANOVA corrected for multiple comparisons). +++: $p<0.0001$ vs. pGL3-empty vector (one-way ANOVA corrected for multiple

comparisons).
(C) Luciferase expression in GripTite 293 MSR cells transfected with different pGL3 luciferase reporters and pCDNA3-GATA1 vectors as indicated. Left: pGL3-intron 8 MYH10 wild-type (WT), pGL3-intron 8 MYH10 mutants, empty pCDNA3 and pCDNA3-GATA1 WT. Middle: pGL3-3'UTR MYH10, empty pCDNA3 and pCDNA3-GATA1 WT. Right: empty pGL3, empty pCDNA and pCDNA-GATA1 WT. The pCDNA3 empty vector was used as a control. *: $p<0.01$, ****: $p<0.0001$ vs. pGL3-intron8-MYH10 WT in the presence of GATA1 (black bar) (one-way ANOVA corrected for multiple comparisons). ++++: $p<0.0001$ vs. the empty pGL3 vector in the absence of GATA1 (white bar). Each plasmid was assayed in six separate transfection experiments (one-way ANOVA corrected for multiple comparisons).
(D) Luciferase expression after transfection in GripTite 293 MSR cells with pGL3-intron 8 MYH10 WT and pCDNA3-GATA1 WT or variant vectors as indicated. *: $p<0.01$ vs. GATA1 WT (one-way ANOVA corrected for multiple comparisons). Each plasmid was assayed in five separate transfection experiments.

Supporting information.

Methods

DNA sequencing, variant calling, variant confirmation and segregation studies

DNA extraction, next-generation sequencing library preparation, variant calling and annotation were performed as previously described [1]. Briefly, the DNA samples were enriched for the exons of 308 genes involved in platelet function and disorders (list available upon request) using HaloPlex technology (Agilent technologies) or SeqCap EZ Choice technology (Roche sequencing). DNA sequencing was then performed on a NextSeq 500 sequencer (Illumina) using 2-channel SBS technology and a Mid-Output kit. Sequence quality was verified using Sequencing Analysis Viewer v1.8.37 software (Illumina). The sequences were then aligned using the Burrows-Wheeler Alignment tool with maximal exact matches (hg19 version of the genome). Variant calling was performed using GATK v3.3.0 and annotated with ANNOVAR [2] and VarAFT software [3]. We applied the following filters for variant analysis: SNPs with a frequency <1% (based on ExAC, 1000G and ESP6500 data), located in coding regions or splice junctions, and designated deleterious by several prediction algorithms (UMD Predictor [4], PROVEAN [5] and Polyphen [6]). We confirmed the variations in probands and pedigree members via Sanger sequencing using a 3500xL Genetic Analyzer.

Structural modeling

Structural modeling of the GATA1 (NP_002040.1) variants was performed using molecular visualization and modeling with Coot and PyMOL software (The PyMOL Molecular Graphics System; Version 1.5.0.4; Schrödinger LLC).

Flow cytometry analysis

Major platelet receptors and granule markers were assessed as previously described [18]. Briefly, PRP samples were incubated either with or without TRAP-14 (Polypeptide group) and antibodies against αIIbβ3 integrin (clone P2, Beckman Coulter), active form of αIIbβ3 (clone PAC-1; BD), GPIbα (clone HIP1, BD Biosciences), CD63 (clone CLB-gran 12; Beckman Coulter) and CD62P (clone CLB-

Thromb/6, BD Biosciences) for 30 min at room temperature. Scatter signals and fluorescence intensity were analyzed using an FC500 Flow Cytometer (Beckman Coulter). Circulating CD34+ cells were quantified as previously reported [27].

Cell expression and luciferase reporter assays

Wild-type *GATA1* cDNA (amplified from pPacGATA1, a gift from Jeffrey W. Taub) [7] was inserted into a pCDNA3.1-cMyc expression vector. The *GATA1* variants were generated using a GENEART Site-directed Mutagenesis System (Life technologies) according to the manufacturer's protocol. The primer sequences used are available upon request. The *MYH10* regulatory regions (intron 8 and the 3' untranslated region [UTR]) were cloned into a pGL3 vector (Proteogenix). Polymerase chain reaction mutagenesis was used to substitute the GATA1 binding sites with an AAAA sequence. The plasmids were denoted M1/M2/M3/M4 when the four binding sites were substituted and M1, M2, M3 or M4 when a single binding site was substituted. After cloning and transformation, each genotype was confirmed using Sanger DNA sequencing (Beckman Coulter Genomics). To examine cell-type dependence, we used the HEL hematopoietic and GripTite 293 MSR (HEK 293 cell line expressing the human macrophage scavenger captor) cell lines. The cells were transfected with pCDNA3.1-cMyc-GATA1 along with the SV40 drive luciferase plasmid (pGL473-hRLuc) to normalize for transfection efficiency. Polyjet (Tebu-bio) was used for transfection according to the manufacturer's protocol. The cells were harvested and lysed 48 hours after transfection. Firefly and Renilla luciferase activity were then measured consecutively using a Dual-Luciferase Reporter 1000 Assay system (Promega) with an EnSight™ Multimode Microplate Reader (PerkinElmer) according to the manufacturer instructions.

PRP serotonin level

PRP was prepared according to standard procedures and then frozen at -70 °C. After thawing and vortexing the sample, the serotonin levels were assessed using high performance liquid chromatography with the following parameters: isocratic flow 0.95 ml/minute, sensor potential 0.5V, sensitivity 10 nA, column temperature 30 ± 1 °C, analysis time 10 minutes, injection volume 20 µl, serotonin retention time 5.2 minutes, eluent retention time 6.8 minutes. The serotonin levels were

then expressed according to the PRP platelet count. The plasma serotonin levels were considered negligible as compared with the intraplatelet serotonin content.

Platelet PA1-1 antigen level

Serum was prepared from blood collected in glass tubes and incubated at 37°C for 120 minutes before centrifugation at 2000 g for 10 minutes at 4°C. The supernatant was stored at -70°C until downstream assays were performed. PAI-1 antigen concentrations in plasma and serum samples were assessed using an enzyme-linked immunosorbent assay (Asserachrom, Diagnostica Stago). The serum results are expressed according to the PRP platelet count after subtracting the plasma values.

Mepacrine uptake and release assay

PRP samples were prepared according to standard procedures and diluted to obtain a platelet concentration of 10^7 platelets/mL. The diluted PRP samples were incubated with 1 µM or 2 µM mepacrine (Q3251, Sigma-Aldrich) for 30 min at 37 °C; diluted control PRP samples were incubated without mepacrine. Next, the platelet samples were incubated either with or without 40 µM TRAP-14. Platelet-mepacrine fluorescence was analyzed using a Navios Cytometer (Beckman Coulter). Mepacrine-labeled dense granules were also quantified via fluorescence microscopy. In single-plane views, mepacrine displayed characteristic punctate staining. A total of 100 platelets were examined, and the number of dense granules per platelet was determined.

Epifluorescence microscopy

Forty-eight hours after transfection, H9C2 cells (ATCC CRL-1446) were fixed in 4% paraformaldehyde for 20 min at room temperature. The cells were then washed, permeabilized with 0.3% Triton X100 in PBS for 5 min, blocked with 3% BSA PBS, and incubated overnight with rabbit anti-cMyc antibody (Santa Cruz Biotechnology; sc-789). Next, the cells were incubated with anti-rabbit Alexa-546-labeled secondary antibody (Life technologies A11010), and DAPI staining was performed. Finally, after washing the cells, the slides were mounted with Fluoromount and examined using an AXIO Imager M1 microscope (Carl Zeiss, Germany).

Platelet lysates, FOG1/GATA1 immunoprecipitation and western blot analysis

The platelet lysates were prepared as previously described.[8] GripTite 293 MSR cells were co-transfected with the vectors pFN21A-halotag-FOG1 (a gift from Dr. Fujiwara)[9] and pCDNA3-cMyc GATA1. Transfected MSR cells were treated with DTBP reagent (Interchim) for crosslinking and lysed with radio-immunoprecipitation assay (RIPA) buffer (Sigma-Aldrich) supplemented with EDTA-free protease cocktail inhibitor (Roche). The immunoprecipitation was carried out overnight at 4°C by incubating the cell extracts with rabbit anti-cMyc coated with magnetic beads (PureProteome, Millipore). After washing the beads with lysis buffer, the immunoprecipitates were suspended in sample loading buffer (NuPAGE LDS sample buffer, Thermo Fisher Scientific) and boiled for 5 min at 95 ºC. The immunoprecipitated proteins were assessed for halotag-FOG1 via western blot.

The proteins were separated on NuPAGE gels with MES SDS running buffer (Thermo Fisher Scientific) and then transferred onto a polyvinylidene fluoride membrane. The membranes were blocked (5% Blotto buffer) and labeled overnight with the following primary antibodies: rabbit anti-MYH10 (Cell Signaling Technology), anti-GATA1 (Thermo Fisher Scientific), mouse anti-halotag (Promega), anti-GPVI, anti-SYK, anti-PLC2, anti-COX, anti-TBXAS, anti-cMyc (Santa-Cruz Biotechnology) and anti-GAPDH (Millipore). The membranes were then incubated with the appropriate horseradish peroxidase-conjugated secondary antibody (Bio-Rad Laboratories). Staining was performed using ECL detection reagent (Life Technologies), and the chemiluminescent blots were imaged using the charge-coupled device camera system ImageQuant LAS 4000 (GE Healthcare) and quantified using ImageJ software (National Institutes of Health, Bethesda, MD, USA).

Supplemental figures

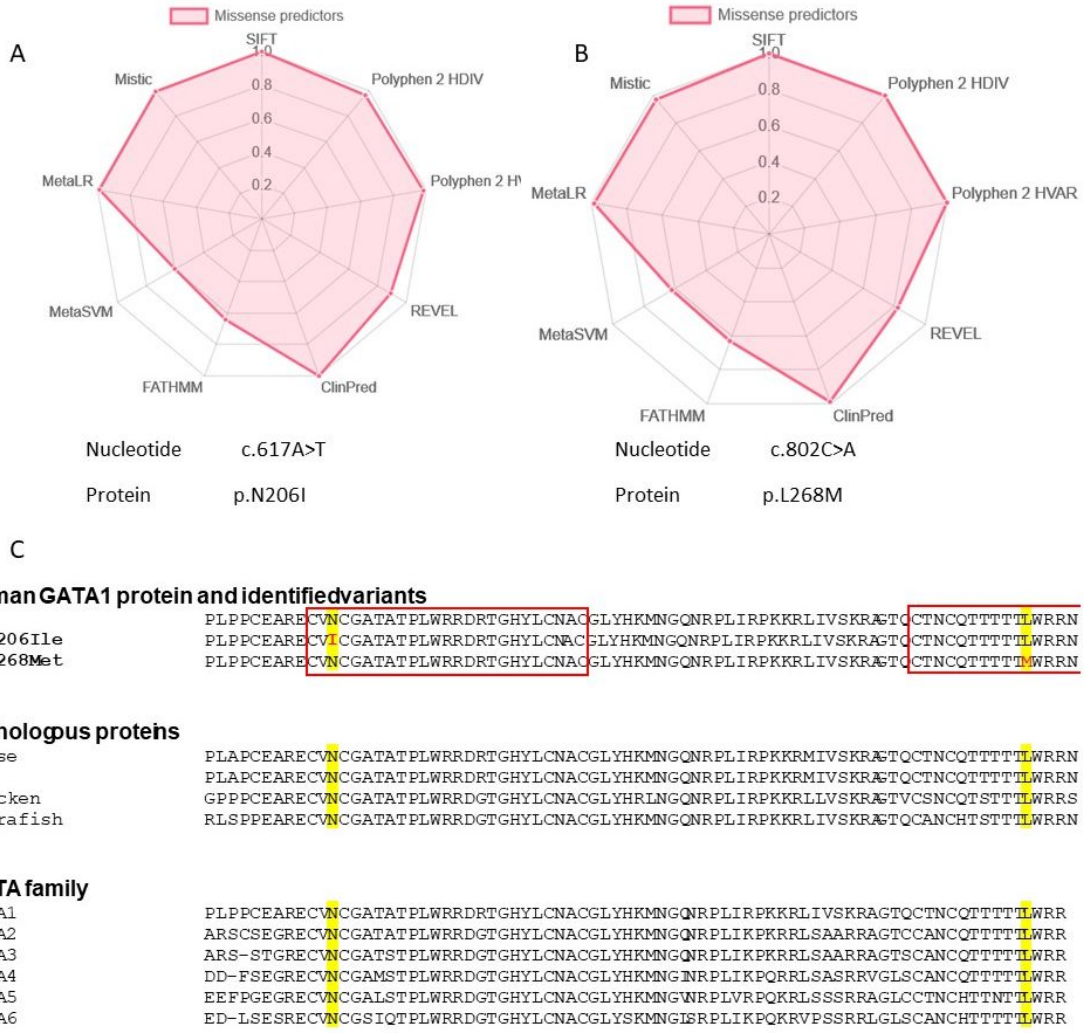

Supplemental Figure 1: Radar view of missense predictors and GATA alignments.
(A-B) Radar view of missense predictors (issued from https://mobidetails.iurc.montp.inserm.fr/MD/). Values are normalized (0-1) 0 being the less damaging and 1 the most for each predictor algorithms. (C) The variants reported in this study are indicated in red (top alignment). Alignments of GATA1 orthologous and different members of the GATA family are provided (middle and bottom alignments, respectively). The boxes delineate both zinc finger domains, ZF1 (position 204-228) and ZF2 (position 258-282). The GATA1 reference variant is NM_002049. WT: wild-type.

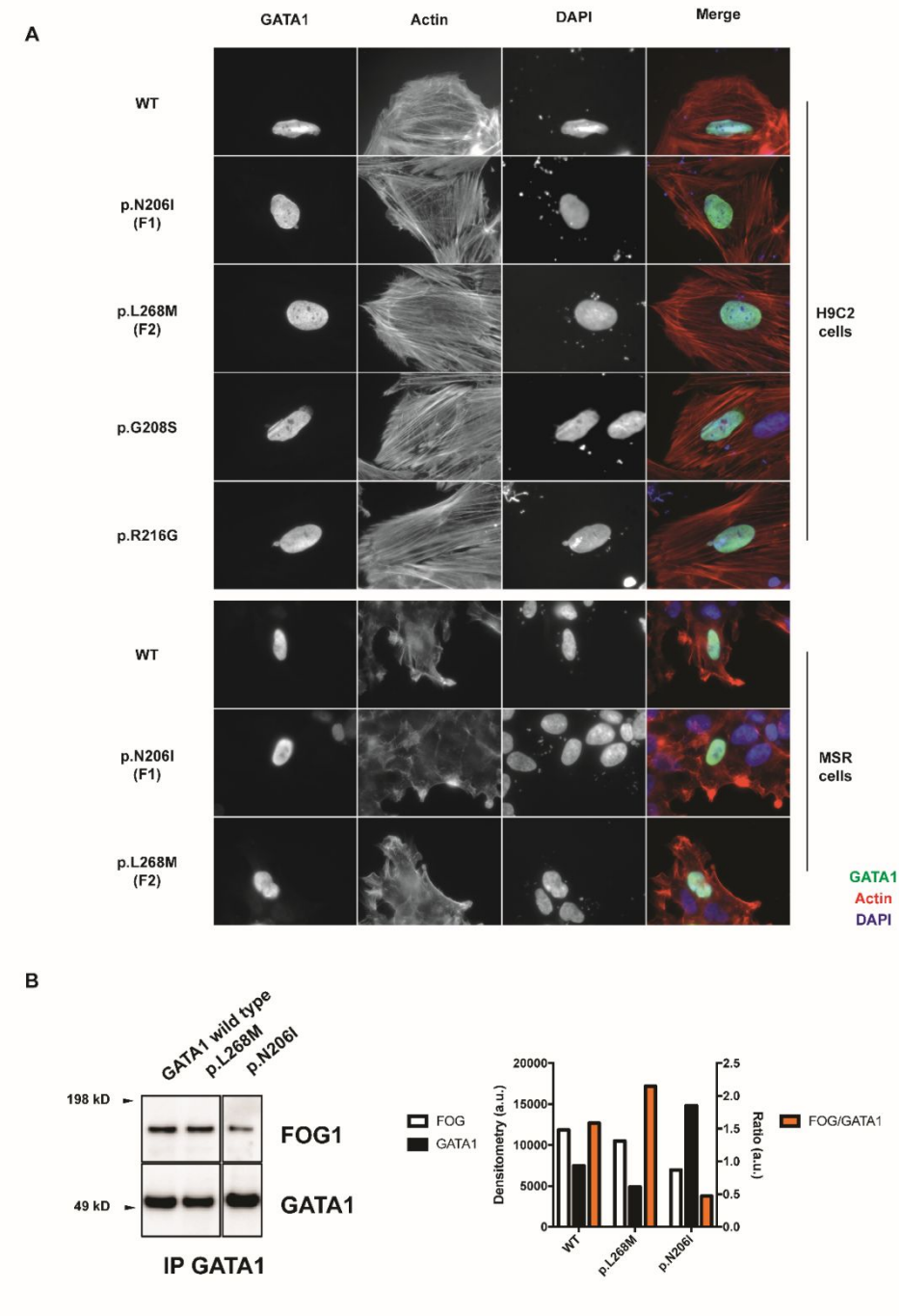

Supplemental Figure 2: Functional characterization of the GATA1 variants.

(A) Subcellular localization of the GATA1 variants. Representative immunofluorescence microscopy images of H9C2 (upper panel) and MSR (lower panel) cells transfected with wild-type (WT) GATA1 or variants (pCDNA3-cMyc-GATA1 expression vectors) after cMyc, actin and DAPI staining (100X magnification). The p.N206I and p.L268M variants were compared to the previously reported variants p.G208S [10] and p.R216G [11,12] as well as WT GATA1.

(B) Immunoprecipitation of GATA1-cMyc in GripTite 293 MSR cells co-transfected with pFN21A-HaloTag-FOG1 and pCDNA3-cMyc GATA1 (wild-type or variants) vectors. Immunoprecipitation was performed on cell lysate with rabbit anti-cMyc antibody (Santa-Cruz, sc-789). The immunoprecipitates

were analyzed via western blot using murine anti-HaloTag (Promega, G921A) and anti-cMyc (Santa-Cruz, sc-40) antibodies. Input correspond to the GATA1 and FOG1 levels before IP. All samples were run together and the bands were detected simultaneously (the original photograph can be provided on request). Quantification of band intensity for FOG1, GATA1 and ratio GOG1/GATA1 is shown to the right of the western blot.

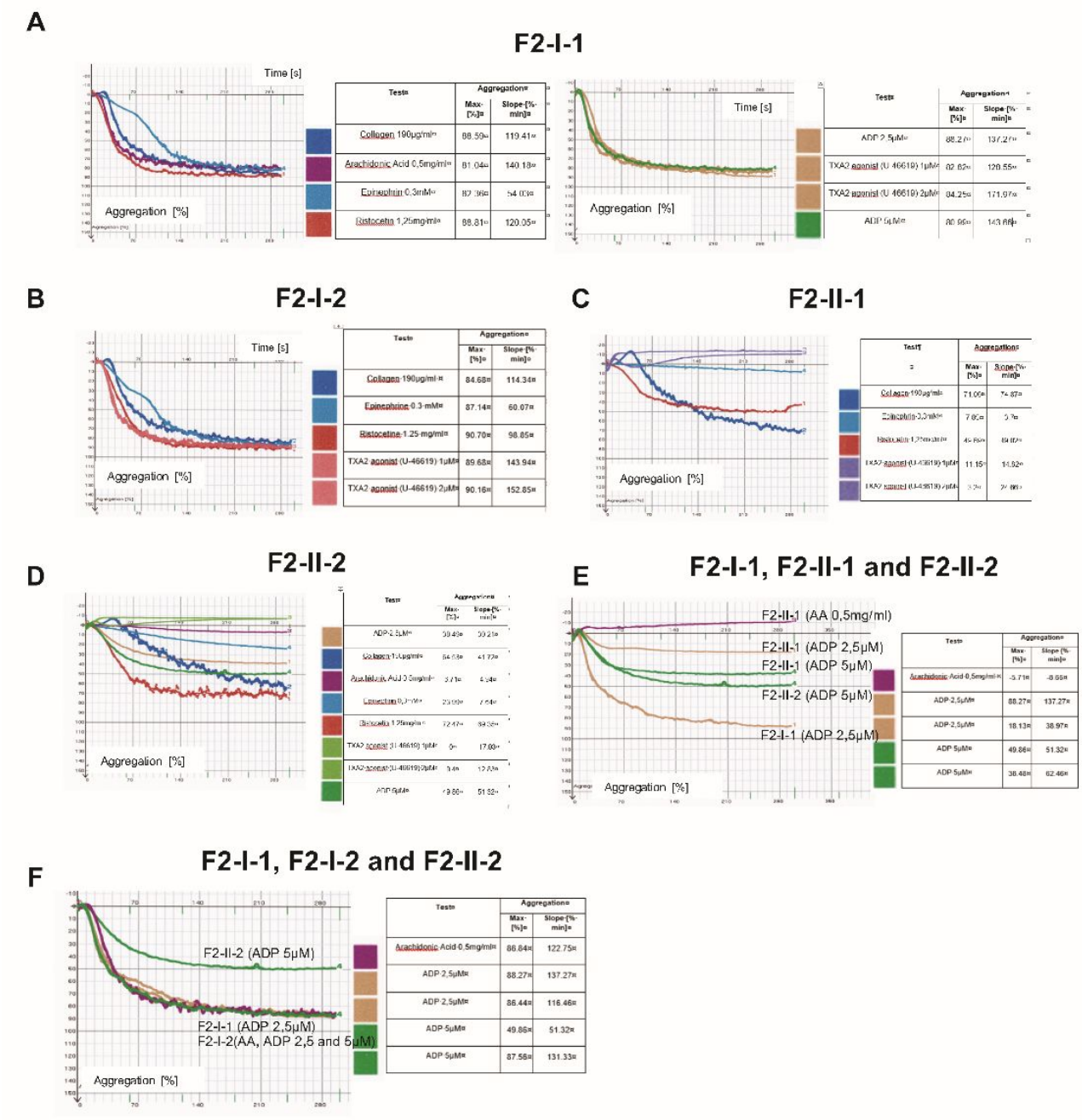

Supplemental Figure 3: Platelet aggregation tracings for F2 family (pL268M).
A-D Aggregation tracings for F2-I-1 (mother), F2-I-2 (father), F2-II-1 (firstborn son) and F2-II-2 (second son) family members, on separated graphs. **E**- Aggregation tracings for F2-I-1, F2-II-1 and F2-II-2 on the same graphs. **F**- Aggregation tracings for F2-I-1, F2-I-2 and F2-II-2 on the same graphs. Platelet aggregation was induced by different agonist and different agonist concentrations indicated in the table, on the right to the curves. Percentage max of aggregation and slope were indicated in the table.

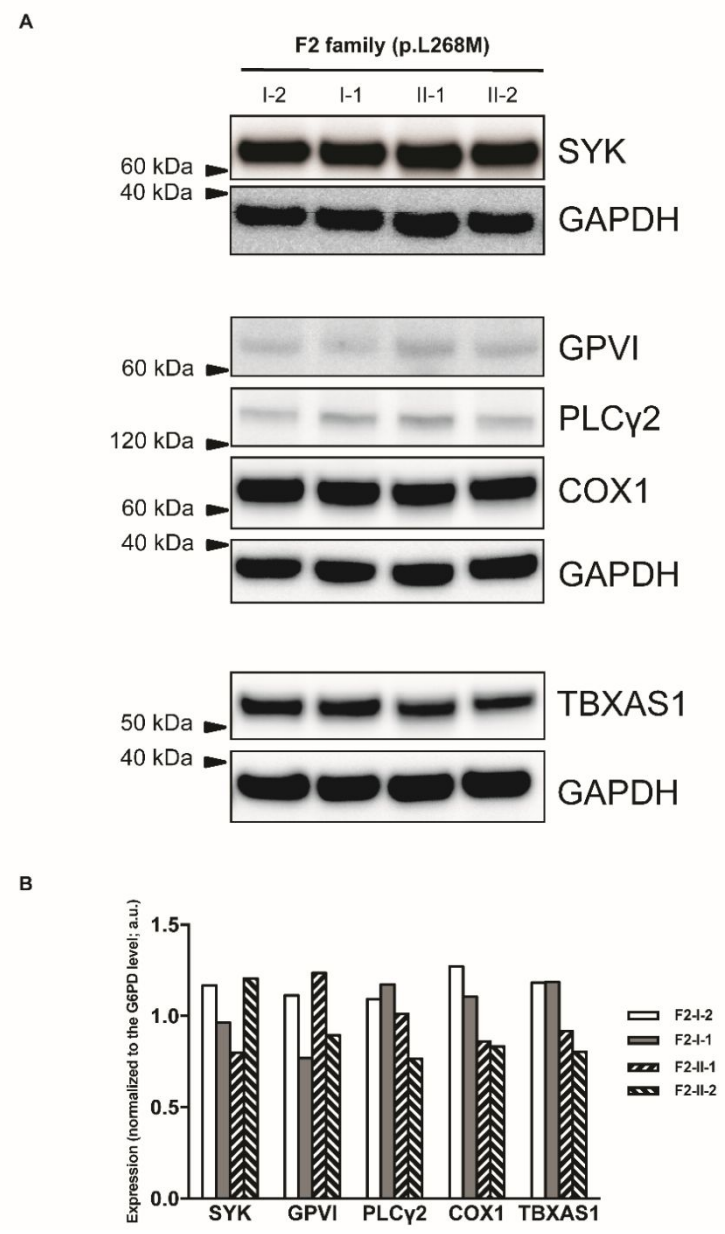

Supplemental

Figure 4: Evaluation of proteins involved in the collagen and arachidonic acid signaling pathways

Expression of the proteins involved in the collagen (GPVI, SYK and PLCγ2) and arachidonic acid (COX, TBXAS1) signaling pathways were analyzed via western blot of platelet lysates (30 µg) from the F2 family members: the GATA1 variant carriers (F2-II-1 and F2-II-2), maternal heterozygous carrier (F2-1-1) and unaffected father (F2-I-2). Quantification of band intensity is shown below the western blots.

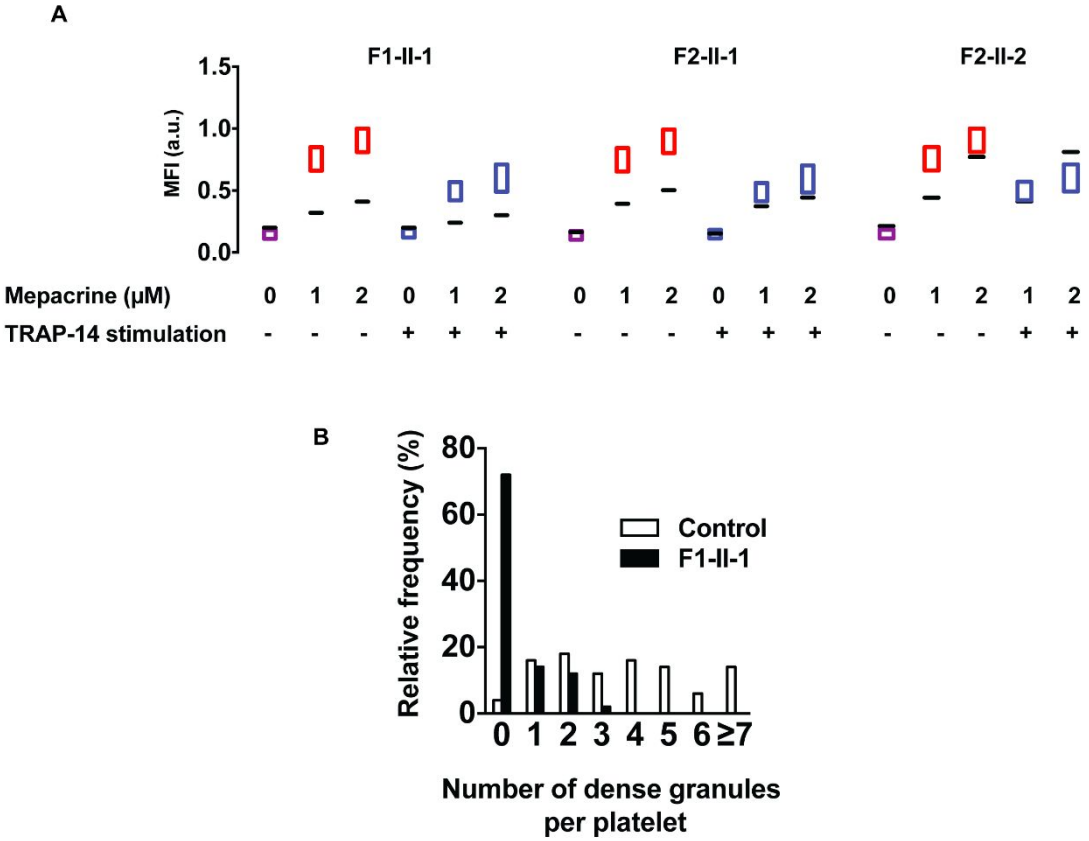

Supplemental Figure 5: Mepacrine test

(A) Flow cytometric mepacrine uptake and release assays of the three variant carriers and unrelated controls. The platelets were incubated with 1 μM or 2 μM mepacrine and stimulated with TRAP-14 (50 μM) to evaluate mepacrine release. Rectangles indicate the reference values, while black horizontal bars indicate the patient values. MFI: mean fluorescence intensity.

(B) Quantification of dense granules in 100 platelets using immunofluorescence microscopy after mepacrine uptake in patient F1-II-1 and a control.

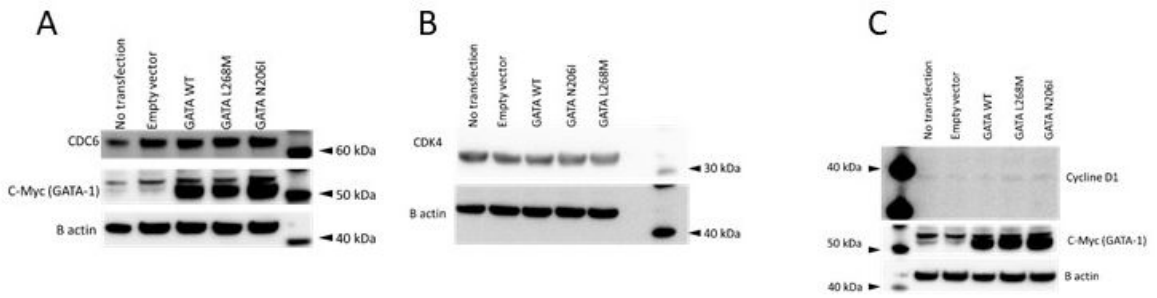

Supplemental Figure 6: Evaluation of proteins involved in GATA-1 mediated polyploidization defect.

Western blot analysis of CDC6 (A), CDK4 (B) and Cyclin-D1 (C) expression in GripTite 293 MSR cell lines transfected with GATA-1 wild-type or variants. GATA-1-cMyc was assessed as a transfection control. Actin expression was assessed as a protein loading control. A and B panels shows the same samples.

3'UTR sequence

hg38_dna range=chr17:8472947-8473157

CAAAGCCCAGCTGCCATAAACTGTCTTCCTTGTGCTCTGAATGCCCAACGAAGGTTGTATAAACTACC
TTTCCTTAGGTCTGGAGTGTCGGGTCAGTCAAGAAGGGACCCTTTTAGTTATTAAATAGTATCTTTGC
AGAATCAGGGCCTGGAATTGGTTCACACAGATTGTTTCTCCTGGCACGCTGAGTAGTTGGGAAACTGT
GACGTGA

Intronic sequence

hg38_dna range=chr17:8553047-8553739

Wild-type

TGGGGCCACCAAAGTAAATTAATTCTGTATGTGTCA***GATA***GCCTGAATTTTAAGTCAGACTA
TCCCACACATCCTCCACGTCTGGTGAAAGACACACTCATATGAATCATGCTCTGACACACCT
ATATGAAGAAAGCTGAACTGCAGATTCATTCTCCTGTCATTTTCAAGTATTTCCAGATTTTG
CTGGCTGTGAGTCCATTTGGAGGCATAAAATACTGTTCTTAACCAGAAAATCATGGTCTGTC
CCTTGAAGGATAGAAATAATGTATTTC***TATC***ACTGGAGATTATTCTATTAAGTACCCGAAAA
CTGTCATC***TATC***TTTCTAATTGGCACAC***TATC***ATTCAGAATCATTTCTATTTTATTACATCT
ATACTCAAATGTGTTTTACCTGGGTATATATGTGCATACACATATATAAACCTTCTTATGGC
CATTCTATGCAGGTGACATTTCTTAGGACTATTCTATGTACTTGACATTTTATTTTTTTCTC
CAGCTTTATTCTACTTAACACTAATTGAGATTACTTTAACTCTGTAATCTTATAAGGATGTT
TTCAATGATTACATGCTCATCCTTCTAATATCAGAAGTAGATGGTAAAAAGTGGGCTAACAG
CAATAGGGGGAGGGCAACTGCATTCATCTGAATGTCCTATATCACACAAACACTGTGGCACT
CTCCACTTCCC

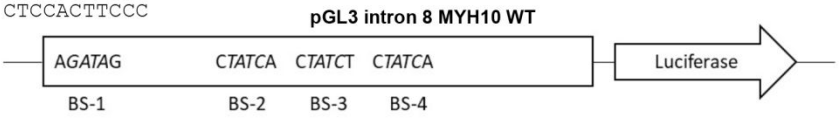

Mutated binding-site (BS-M1,2,3,4)

TGGGGCCACCAAAGTAAATTAATTCTGTATGTGTCA***AAAA***GCCTGAATTTTAAGTCAGACTA
TCCCACACATCCTCCACGTCTGGTGAAAGACACACTCATATGAATCATGCTCTGACACACCT
ATATGAAGAAAGCTGAACTGCAGATTCATTCTCCTGTCATTTTCAAGTATTTCCAGATTTTG
CTGGCTGTGAGTCCATTTGGAGGCATAAAATACTGTTCTTAACCAGAAAATCATGGTCTGTC
CCTTGAAGGATAGAAATAATGTATTTC***AAAA***ACTGGAGATTATTCTATTAAGTACCCGAAAA
CTGTCATC***AAAA***TTTCTAATTGGCACAC***AAAA***ATTCAGAATCATTTCTATTTTATTACATCT
ATACTCAAATGTGTTTTACCTGGGTATATATGTGCATACACATATATAAACCTTCTTATGGC
CATTCTATGCAGGTGACATTTCTTAGGACTATTCTATGTACTTGACATTTTATTTTTTTCTC
CAGCTTTATTCTACTTAACACTAATTGAGATTACTTTAACTCTGTAATCTTATAAGGATGTT
TTCAATGATTACATGCTCATCCTTCTAATATCAGAAGTAGATGGTAAAAAGTGGGCTAACAG
CAATAGGGGGAGGGCAACTGCATTCATCTGAATGTCCTATATCACACAAACACTGTGGCACT
CTCCACTTCCC

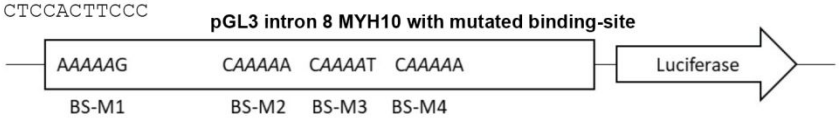

Supplemental Figure 7: DNA sequence of regulatory GATA1 binding regions of the MYH10 gene.

The sequences of the 3'UTR (Chr. 17: 8472947-8473157) and intronic region (Chr. 17: 8553047-8553739) of the MYH10 gene. The putative consensus binding sites for GATA1 within intron 8 of the MYH10 gene are displayed in italic and underlined in green. Both fragments were cloned into a luciferase construct, 5' of the luciferase reporter gene, to generate pGL3-3'UTR MYH10 WT and pGL3-Intron 8 MYH10 WT. The binding-site mutant constructs are pGL3-Intron 8 MYH10 M1, pGL3-Intron 8 MYH10 M2, pGL3-Intron 8 MYH10 M3, pGL3-Intron 8 MYH10 M4 and pGL3-Intron 8 MYH10 M(1,2,3,4) with the indicated mutations.

Supplemental Figure 8: FLI1, RUNX1 and GATA1 transcription factor cell expression

Western blot analysis of FLI1, RUNX1 and GATA1 expression in native (non-transfected, NT) HEL cells, native GripTite 293 MSR cell lines, and transfected (with RUNX1, FLI1 or GATA1) GripTite 293 MSR cell lines. GAPDH expression was assessed as a protein loading control.

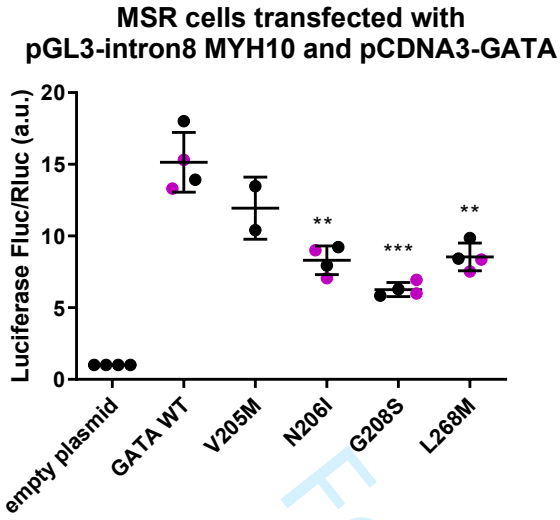

Supplemental Figure 9: Functional analysis of the MYH10 regulatory regions.
Luciferase expression after transfection in GripTite 293 MSR cells with pGL3-intron 8 MYH10 WT and pCDNA3-GATA1 WT or variant vectors as indicated. ** p<0.01 vs. GATA1 WT (one-way ANOVA corrected for multiple comparisons). Each plasmid was assayed in duplicate in one or two separate transfection experiments (pink or black symbols).

Supplemental Table 1 Candidate genes

Gene	Variation (NM)	gnomAD exome (v2.0.1 Exomes global MAF)	gnomAD genome (Genomes global MAF)	gnomAD (v3 Genomes global MAF)	dbSNP rsid (*Identifier for NCBI dbSNP*)	Clinvar interpretation (v20210123)	CADD raw: *[-6.41;35.5] The higher the less likely to be observed*	CADD phred *Phred-like scaling of raw score*	MPA score *Raw score [0;10], 10: high impact*	MPA impact
WDR66	c.1915C>T (NM_144668.5)	0.0001	9.686e-05	8.373e-05	rs202238684	No match	6.3	35	10	Nonsense
LYST	c.11268-5del (NM_000081.3)(	0.5087	0.5810	0.5679	No match	Benign / Likely benign	0.079599	1.915	0	Unknown
GCKR	c.217-8C>T (NM_001486.3)	0.0001	No match	2.791e-05	rs755995385	No match	0.26	3.88	0	Unknown
CD226	c.-33delT (NM_001303618.1)	0.0117	0.0089	0.0091	rs3214811	No match	0.017666	1.450	0	Unknown
RNF145	c.1270-9_1270-4del (NM_001199383.1)	0.0015	0.0014	0.0017	rs59997682	No match	0.704591	8.497	0	Unknown

Supplemental Table 2 Morphometric parameters from sections of platelet electron microscopy.

See the Methods section for the comparison between the patient and the controls

	Platelet area (μm^2)	Major platelet diameter (μm)	Minor platelet diameter (μm)	Alpha granule diameter (nm)	Alpha granule per μm^2
Controls (n=10)	2.79±1.60	2.85±1.23	1.25±1.49	235±1.2	2.51±1.29
F2-II-1	2.74±1.73	2.75±1.26	1.27±1.51	208±1.4	1.08±0.81
p-value	*0.751*	*0.104*	*0.663*	*<0.001*	*<0.001*

Supplemental references

1 Saultier P, Vidal L, Canault M, Bernot D, Falaise C, Pouymayou C, Bordet J-C, Saut N, Rostan A, Baccini V, Peiretti F, Favier M, Lucca P, Deleuze J-F, Olaso R, Boland A, Morange PE, Gachet C, Malergue F, Fauré S, et al. Macrothrombocytopenia and dense granule deficiency associated with FLI1 variants: ultrastructural and pathogenic features. *Haematologica* 2017; **102**: 1006–16.

2 Wang K, Li M, Hakonarson H. ANNOVAR: functional annotation of genetic variants from high-throughput sequencing data. *Nucleic Acids Res* 2010; **38**: e164.

3 Desvignes J-P, Bartoli M, Delague V, Krahn M, Miltgen M, Béroud C, Salgado D. VarAFT: a variant annotation and filtration system for human next generation sequencing data. *Nucleic Acids Res* 2018; **46**: W545–53.

4 Frédéric MY, Lalande M, Boileau C, Hamroun D, Claustres M, Béroud C, Collod-Béroud G. UMD-predictor, a new prediction tool for nucleotide substitution pathogenicity -- application to four genes: FBN1, FBN2, TGFBR1, and TGFBR2. *Hum Mutat* 2009; **30**: 952–9.

5 Choi Y, Sims GE, Murphy S, Miller JR, Chan AP. Predicting the functional effect of amino acid substitutions and indels. *PLoS ONE* 2012; **7**: e46688.

6 Adzhubei IA, Schmidt S, Peshkin L, Ramensky VE, Gerasimova A, Bork P, Kondrashov AS, Sunyaev SR. A method and server for predicting damaging missense mutations. *Nat Methods* 2010; **7**: 248–9.

7 Caldwell JT, Edwards H, Dombkowski AA, Buck SA, Matherly LH, Ge Y, Taub JW. Overexpression of GATA1 confers resistance to chemotherapy in acute megakaryocytic Leukemia. *PLoS ONE* 2013; **8**: e68601.

8 Poggi M, Canault M, Favier M, Turro E, Saultier P, Ghalloussi D, Baccini V, Vidal L, Mezzapesa A, Chelghoum N, Mohand-Oumoussa B, Falaise C, Favier R, Ouwehand WH, Fiore M, Peiretti F, Morange PE, Saut N, Bernot D, Greinacher A, et al. Germline variants in ETV6 underlie reduced platelet formation, platelet dysfunction and increased levels of circulating CD34+ progenitors. *Haematologica* 2017; **102**: 282–94.

9 Fujiwara T, Sasaki K, Saito K, Hatta S, Ichikawa S, Kobayashi M, Okitsu Y, Fukuhara N, Onishi Y, Harigae H. Forced FOG1 expression in erythroleukemia cells: Induction of erythroid genes and repression of myelo-lymphoid transcription factor PU.1. *Biochem Biophys Res Commun* 2017; **485**: 380–7.

10 Mehaffey MG, Newton AL, Gandhi MJ, Crossley M, Drachman JG. X-linked thrombocytopenia caused by a novel mutation of GATA-1. *Blood* 2001; **98**: 2681–8.

11 Yu C, Niakan KK, Matsushita M, Stamatoyannopoulos G, Orkin SH, Raskind WH. X-linked thrombocytopenia with thalassemia from a mutation in the amino finger of GATA-1 affecting DNA binding rather than FOG-1 interaction. *Blood* 2002; **100**: 2040–5.

12 Balduini CL, Pecci A, Loffredo G, Izzo P, Noris P, Grosso M, Bergamaschi G, Rosti V, Magrini U, Ceresa IF, Conti V, Poggi V, Savoia A. Effects of the R216Q mutation of GATA-1 on erythropoiesis and megakaryocytopoiesis. *Thromb Haemost* 2004; **91**: 129–40.